JACS
JOURNAL OF THE AMERICAN CHEMICAL SOCIETY

ARTICLE

pubs.acs.org/JACS

Electrocatalytic Oxidation of Formate by $[Ni(P^R_2N^{R'}_2)_2(CH_3CN)]^{2+}$ Complexes

Brandon R. Galan,[‡] Julia Schöffel,[†] John C. Linehan,[‡] Candace Seu,[†] Aaron M. Appel,*[,‡] John A. S. Roberts,[‡] Monte L. Helm,[#] Uriah J. Kilgore,[‡] Jenny Y. Yang,[‡] Daniel L. DuBois,[‡] and Clifford P. Kubiak*[,†]

[‡]Chemical and Materials Sciences Division, Pacific Northwest National Laboratory, Richland, Washington 99352, United States

[†]Department of Chemistry & Biochemistry, University of California, San Diego, 9500 Gilman Drive, La Jolla, California 02093, United States

[#]Chemistry Department, Fort Lewis College, 1000 Rim Drive, Durango, Colorado 81301, United States

Supporting Information

ABSTRACT: $[Ni(P^R_2N^{R'}_2)_2(CH_3CN)]^{2+}$ complexes with R = Ph, R′ = 4-MeOPh or R = Cy, R′ = Ph , and a mixed-ligand $[Ni(P^R_2N^{R'}_2)(P^{R''}_2N^{R'}_2)(CH_3CN)]^{2+}$ with R = Cy, R′ = Ph, R″ = Ph, have been synthesized and characterized by single-crystal X-ray crystallography. These and previously reported complexes are shown to be electrocatalysts for the oxidation of formate in solution to produce CO_2, protons, and electrons, with rates that are first-order in catalyst and formate at formate concentrations below ~0.04 M (34 equiv). At concentrations above ~0.06 M formate (52 equiv), catalytic rates become nearly independent of formate concentration. For the catalysts studied, maximum observed turnover frequencies vary from <1.1 to 15.8 s^{-1} at room temperature, which are the highest rates yet reported for formate oxidation by homogeneous catalysts. These catalysts are the only base-metal electrocatalysts as well as the only homogeneous electrocatalysts reported to date for the oxidation of formate. An acetate complex demonstrating an η^1-$OC(O)CH_3$ binding mode to nickel has also been synthesized and characterized by single-crystal X-ray crystallography. Based on this structure and the electrochemical and spectroscopic data, a mechanistic scheme for electrocatalytic formate oxidation is proposed which involves formate binding followed by a rate-limiting proton and two-electron transfer step accompanied by CO_2 liberation. The pendant amines have been demonstrated to be essential for electrocatalysis, as no activity toward formate oxidation was observed for the similar $[Ni(depe)_2]^{2+}$ (depe = 1,2-bis(diethylphosphino)ethane) complex.

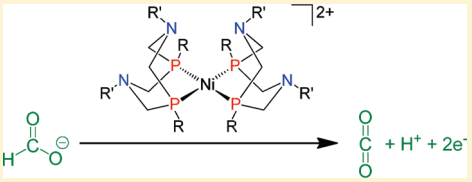

INTRODUCTION

The temporal variation in the availability of renewable energy sources such as solar and wind makes storage of this energy in the form of fuels attractive.[1] Water-splitting is one attractive route for energy storage, but the low volumetric energy density of H_2 has motivated efforts to store energy in the form of reduced carbon products with much higher volumetric energy densities, such as methanol or formic acid. Although formic acid has a lower energy density than methanol, current formic acid fuel cells can run at much higher concentrations than methanol fuel cells, with the result that the performance of formic acid fuel cells is competitive with the performance of methanol fuel cells.[2−4]

Currently formic acid is mainly produced by carbonylation of methanol followed by hydrolysis.[5] However, there is also much current work on the production of formic acid by direct electrochemical reduction of carbon dioxide or indirectly via water electrolysis to form hydrogen followed by hydrogenation of CO_2 to produce formic acid.[6−8] Once viable methods become available for producing formic acid for energy storage, electrocatalysts for the oxidation of formic acid will be of interest. At present, however, the only electrocatalysts reported for this process are heterogeneous catalysts based upon precious metals such as platinum, palladium, or rhodium.[9−17]

One possible pathway for formate oxidation involves the heterolytic cleavage of the C−H bond. Recent work in one of our laboratories has shown that $[Ni(P^R_2N^{R'}_2)_2(CH_3CN)]^{2+}$ complexes rapidly and reversibly promote the heterolytic cleavage of H_2 into a hydride and proton during H_2 oxidation using the nickel center as a hydride acceptor and the ligand as a proton acceptor. There is also a considerable body of information on the factors controlling the hydride acceptor abilities of this class of complexes.[9,10] In fact, metal diphosphine complexes were used to determine the hydride donor ability of formate in acetonitrile solutions (44 ± 2 kcal/mol),[11] and this transfer of a hydride from formate to generate CO_2 and a metal hydride can be viewed as the first step in the oxidation of formate. It was anticipated that $[Ni(P^R_2N^{R'}_2)_2(CH_3CN)]^{2+}$ complexes would be electrocatalysts for formate oxidation, as the hydride acceptor ability of $[Ni(P^R_2N^{R'}_2)_2(CH_3CN)]^{2+}$ complexes is in the appropriate range to accept a hydride from formate and can be systematically varied, and because the pendant bases can facilitate the oxidation of hydrides to protons.

Received: May 16, 2011
Published: June 21, 2011

Chart 1

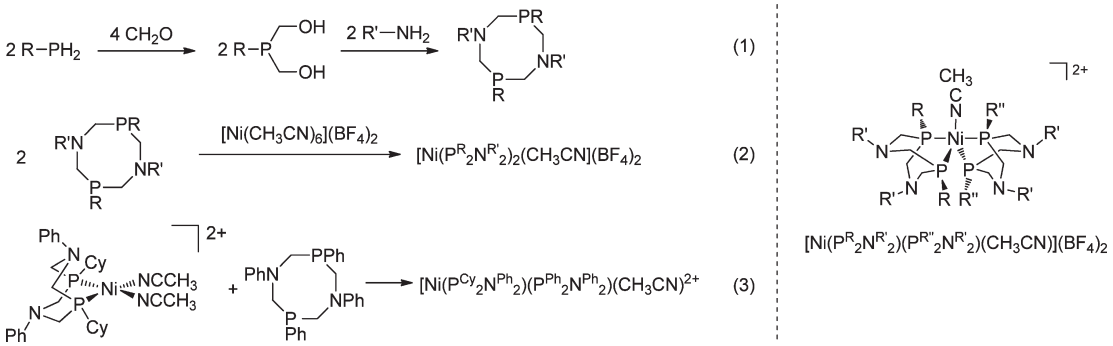

In this article we examine the influence of different phosphorus and nitrogen substituents of $[Ni(P^{R}_2N^{R'}_2)_2(CH_3CN)]^{2+}$ complexes for catalytic formate oxidation and the role of a pendant base in this electrocatalytic process. The synthesis and characterization of new $[Ni(P^{R}_2N^{R'}_2)_2(CH_3CN)]^{2+}$ complexes are described. The formation of nickel hydride species by reaction with hydrogen as well as with formate is also described, and the hydride donor abilities ($\Delta G^{\circ}_{H^-}$) of three new hydride complexes are reported. Finally, the activities for electrocatalytic oxidation of formate are discussed, both for the new complexes reported here as well as for previously reported complexes.

RESULTS

Synthesis and Characterization of Ligands and Complexes. The ligands used for this study differ in the substitution on the phosphorus (R) and the nitrogen atoms (R′) of the eight-membered ring of the $P^{R}_2N^{R'}_2$ ligands, as shown in eq 1 in Chart 1. The synthesis of the ligands was performed according to literature procedures.[12−15] The ligands used in this study were the following: $P^{Ph}_2N^{PhOMe}_2$ (1,5-di(4-methoxyphenyl)-3,7-diphenyl-1,5-diaza-3,7-diphosphacyclooctane), $P^{Ph}_2N^{Ph}_2$ (1,3,5,7-tetraphenyl-1,5-diaza-3,7-diphosphacyclooctane), and $P^{Cy}_2N^{Ph}_2$ (1,5-diphenyl-3,7-dicyclohexyl-1,5-diaza-3,7-diphosphacyclooctane). Using these ligands, the two homoleptic complexes, $[Ni(P^{Ph}_2N^{PhOMe}_2)_2(CH_3CN)](BF_4)_2$ and $[Ni(P^{Cy}_2N^{Ph}_2)_2(CH_3CN)](BF_4)_2$, were prepared by the reaction of $[Ni(CH_3CN)_6](BF_4)_2$ in acetonitrile with 2 equiv of the ligand, as shown in eq 2 in Chart 1.[12] A heteroleptic complex was prepared in two steps. First, the complex $[Ni(P^{Cy}_2N^{Ph}_2)(CH_3CN)_2](BF_4)_2$ was prepared by the reaction of $[Ni(CH_3CN)_6](BF_4)_2$ and 1 equiv of the ligand $P^{Cy}_2N^{Ph}_2$ in acetonitrile. After isolation of the intermediate $[Ni(P^{Cy}_2N^{Ph}_2)(CH_3CN)_2](BF_4)_2$, the second ligand, $P^{Ph}_2N^{Ph}_2$, was coordinated in a second step (eq 3 in Chart 1), yielding the mixed complex $[Ni(P^{Cy}_2N^{Ph}_2)(P^{Ph}_2N^{Ph}_2)(CH_3CN)](BF_4)_2$. The spectroscopic data are consistent with reports of other homo- and heteroleptic nickel complexes with phosphine ligands and are provided in the Experimental Section. These four complexes, $[Ni(P^{Ph}_2N^{PhOMe}_2)_2(CH_3CN)](BF_4)_2$, $[Ni(P^{Cy}_2N^{Ph}_2)_2(CH_3CN)](BF_4)_2$, $[Ni(P^{Cy}_2N^{Ph}_2)(CH_3CN)_2](BF_4)_2$, and $[Ni(P^{Cy}_2N^{Ph}_2)(P^{Ph}_2N^{Ph}_2)(CH_3CN)](BF_4)_2$, were also characterized by X-ray diffraction studies, as discussed below.

In order to explore the reactivities of the $Ni(P_2N_2)_2^{2+}$ complexes, an acetonitrile- and benzonitrile-soluble source of formate or formic acid was required. Aqueous formic acid was avoided due to immiscibility of water with benzonitrile, as well as the potential variability of electrocatalytic rates with water concentration, as recently reported elsewhere.[16] A well-behaved, acetonitrile- and benzonitrile-soluble solid was ultimately isolated by starting from aqueous tetrabutylammonium hydroxide and aqueous formic acid, followed by extraction into ethyl acetate and then crystallization. The product of this reaction was found to be a 1:1 mixture of tetrabutylammonium formate and formic acid, noted as $NBu_4HCO_2 \cdot HCO_2H$. Elemental analysis and ^{1}H NMR spectroscopy are consistent with this assignment, and a single-crystal X-ray structure was collected and is in the Supporting Information. Each formate and formic acid pair share one proton, which appears at 18.7 ppm in the ^{1}H NMR spectrum in CD_3CN. This solid, crystalline material was used as the source of formate/formic acid for the reactions reported here.

Complexes $[Ni(P^{Ph}_2N^{PhOMe}_2)_2(CH_3CN)]^{2+}$, $[Ni(P^{Cy}_2N^{Ph}_2)_2(CH_3CN)]^{2+}$, and $[Ni(P^{Cy}_2N^{Ph}_2)(P^{Ph}_2N^{Ph}_2)(CH_3CN)]^{2+}$ react with $NBu_4HCO_2 \cdot HCO_2H$ to form the respective nickel hydride complexes, $[HNi(P^{Ph}_2N^{PhOMe}_2)_2]^+$, $[HNi(P^{Cy}_2N^{Ph}_2)_2]^+$, and $[HNi(P^{Cy}_2N^{Ph}_2)(P^{Ph}_2N^{Ph}_2)]^+$. Formation of the hydride species was confirmed by new signals in the $^{31}P\{^1H\}$ NMR spectra and the presence of unambiguous hydride signals between −8 and −11 ppm in the ^{1}H NMR spectra (see Supporting Information for the ^{31}P NMR spectra and a discussion of the ^{1}H NMR spectra for the hydride resonances). These hydride complexes are unstable in solution under a nitrogen or argon atmosphere. After 1 week, an acetonitrile solution of $[HNi(P^{Ph}_2N^{PhOMe}_2)_2]^+$ forms a colorless precipitate, and the color of the solution changes from yellow to red. The red color is attributed to the formation of the starting complex $[Ni^{II}(P^{Ph}_2N^{PhOMe}_2)_2(CH_3CN)]^{2+}$, while the precipitate is the nickel(0) complex, $[Ni^0(P^{Ph}_2N^{PhOMe}_2)_2]$ (both confirmed by $^{31}P\{^1H\}$ NMR). This nickel(0) complex $[Ni^0(P^{Ph}_2N^{PhOMe}_2)_2]$ was synthesized and isolated independently by the reaction of $[Ni^{II}(P^{Ph}_2N^{PhOMe}_2)_2(CH_3CN)]^{2+}$ with an excess of formate or by reaction with 2 equiv of $NaB(OMe)_3H$. The spectral data for $[Ni^0(P^{Ph}_2N^{PhOMe}_2)_2]$ are provided in the Experimental Section section, and the crystal structure is shown below. Complexes $[HNi(P^{Cy}_2N^{Ph}_2)_2]^+$ and $[HNi(P^{Cy}_2N^{Ph}_2)(P^{Ph}_2N^{Ph}_2)]^+$ exhibit similar behavior to $[HNi(P^{Ph}_2N^{PhOMe}_2)_2]^+$. This disproportionation reaction is presumably accompanied by the formation of hydrogen gas as shown in eq 4.

$$2[HNi^{II}(P^{Ph}_2N^{PhOMe}_2)_2]^+ \xrightarrow[1\ \text{week}]{CH_3CN} [Ni^{II}(P^{Ph}_2N^{PhOMe}_2)_2]^{2+} + [Ni^0(P^{Ph}_2N^{PhOMe}_2)_2] + H_2 \quad (4)$$

dx.doi.org/10.1021/ja204489e |J. Am. Chem. Soc. 2011, 133, 12767–12779

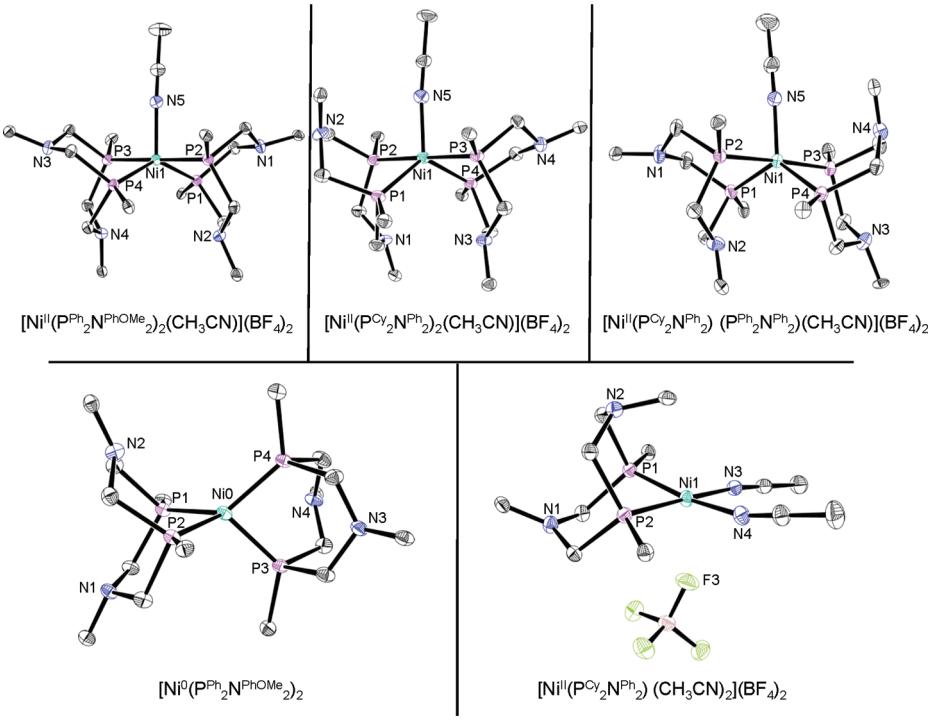

Figure 1. Thermal ellipsoid plots of the crystal structures of the complexes. Thermal ellipsoids are shown at the 50% probability level. For clarity, hydrogen atoms and uncoordinated counterions and solvent molecules are omitted, and only the first carbon of the nitrogen and phosphorus substituents are shown: $[Ni(P^{Ph}_2N^{PhOMe}_2)_2(CH_3CN)](BF_4)_2 \cdot CH_3CN$; $[Ni(P^{Cy}_2N^{Ph}_2)_2(CH_3CN)](BF_4)_2$; $[Ni(P^{Cy}_2N^{Ph}_2)(P^{Ph}_2N^{Ph}_2)(CH_3CN)](BF_4)_2 \cdot 3/8\ Et_2O$, where P(1) and P(2) belong to the $P^{Ph}_2N^{Ph}_2$ ligand and P(3) and P(4) belong to the $P^{Cy}_2N^{Ph}_2$ ligand; $[Ni(P^{Ph}_2N^{PhOMe}_2)_2] \cdot THF$; and $[Ni(P^{Cy}_2N^{Ph}_2)(CH_3CN)_2](BF_4)_2 \cdot CH_3CN$.

X-ray Diffraction Studies. Crystal structures of the four dicationic complexes $[Ni(P^{Ph}_2N^{PhOMe}_2)_2(CH_3CN)](BF_4)_2$, $[Ni(P^{Cy}_2N^{Ph}_2)_2(CH_3CN)](BF_4)_2$, $[Ni(P^{Cy}_2N^{Ph}_2)(CH_3CN)_2](BF_4)_2$, and $[Ni(P^{Cy}_2N^{Ph}_2)(P^{Ph}_2N^{Ph}_2)(CH_3CN)](BF_4)_2$ as well as the structure of the neutral complex $[Ni(P^{Ph}_2N^{PhOMe}_2)_2]$ were obtained, as shown in Figure 1, and selected bond lengths and angles are in the Supporting Information. The crystals of the three nickel(II) bis-diphosphine complexes were all grown from acetonitrile solutions of the complexes layered with diethyl ether at −35 °C. All three structures show a trigonal bipyramidal coordination geometry around the nickel(II) center. In each of these complexes, both P_2N_2 ligands are coordinated via the phosphorus donor atoms to axial and equatorial positions on the nickel(II). The third equatorial ligand is an acetonitrile molecule. The bond lengths and angles, as well as the bite angles, are comparable to those of previously reported structures,[12] but there are some differences in the boat/chair conformations of the rings, likely due to packing effects.

The structure of the zero-valent complex $[Ni(P^{Ph}_2N^{PhOMe}_2)_2]$ was determined with crystals grown from vapor diffusion of pentane into a THF solution of the complex at −35 °C. As expected for a nickel(0) complex, the structure shows a tetrahedral coordination geometry. The same coordination geometry was observed for the recently published $[Ni(P^{Ph}_2N^{Me}_2)_2]$ complex, and in fact, the bond lengths and angles are very similar to those reported in the literature.[17]

Crystals of $[Ni(P^{Cy}_2N^{Ph}_2)(CH_3CN)_2](BF_4)_2$ suitable for X-ray diffraction were grown from an acetonitrile solution of the compound layered with diethyl ether at room temperature. The structure can be described as a distorted square planar coordination geometry around the nickel center. The square plane is spanned by the two phosphorus atoms of the $P^{Cy}_2N^{Ph}_2$ ligand and two nitrogen atoms of two coordinated acetonitrile molecules. Selected bond lengths and angles are in the Supporting Information.

The nickel η^1-acetate complex, $[Ni(P^{Ph}_2N^{Bn}_2)_2(OAc)](BF_4)$ (Bn = benzyl), was synthesized by adding 1 equiv of tetrabutylammonium acetate (NBu_4OAc) to a solution of $[Ni(P^{Ph}_2N^{Bn}_2)_2(CH_3CN)](BF_4)_2$ (synthesized as previously described)[9] in

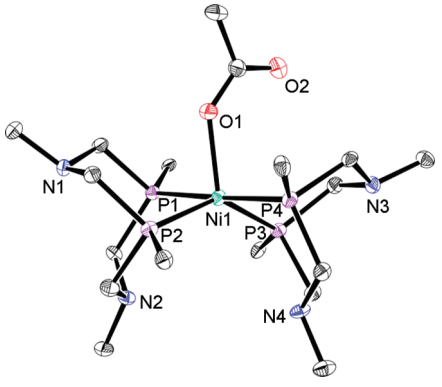

Figure 2. Perspective thermal ellipsoid plot of the crystal structure of $[Ni(P^{Ph}_2N^{Bn}_2)_2(OAc)](BF_4)$. Thermal ellipsoids are shown at the 50% probability level. The Ni1−O1 distance is 2.09 Å, whereas Ni1−O2 is 3.56 Å. For clarity, hydrogen atoms and uncoordinated counterions are omitted, and only the first carbon of the nitrogen and phosphorus substituents is shown.

dx.doi.org/10.1021/ja204489e |J. Am. Chem. Soc. 2011, 133, 12767–12779

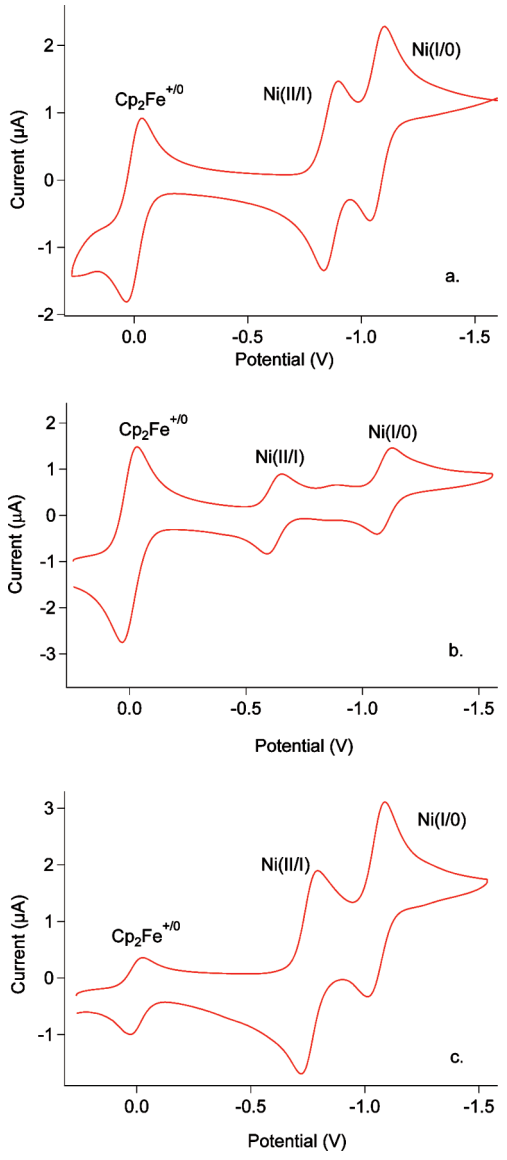

Figure 3. Cyclic voltammograms of (a) $[Ni(P^{Ph}{}_2N^{PhOMe}{}_2)_2(CH_3CN)]^{2+}$, (b) $[Ni(P^{Cy}{}_2N^{Ph}{}_2)_2(CH_3CN)]^{2+}$, and (c) $[Ni(P^{Cy}{}_2N^{Ph}{}_2)(P^{Ph}{}_2N^{Ph}{}_2)(CH_3CN)]^{2+}$ Conditions: 0.8 mM solutions of the complexes in acetonitrile, 0.2 M NBu_4OTf as supporting electrolyte, glassy carbon working electrode, scan rate of 50 mV/s. The cyclic voltammogram for $[Ni(P^{Cy}{}_2N^{Ph}{}_2)_2(CH_3CN)]^{2+}$ was recorded in a 20% benzonitrile/acetonitrile solution. Potentials are referenced with respect to the ferrocenium/ferrocene couple.

benzonitrile. The complex crystallizes as a distorted trigonal bipyramid with the acetate bound through a single oxygen in the equatorial plane, as shown in Figure 2. Bond distances and angles are shown in the Supporting Information. The trigonal plane is distorted, with one oxygen−nickel−phosphine angle being 122.05° and the other angle being 99.58°. There are no known structures of analogous nickel(II) tetraphosphine acetate complexes with which to compare directly. However, the Ni−O bond length of 2.092 Å is slightly longer (2.055 and 2.050 Å) than those of other nickel(II) acetate complexes in the literature,[18−21] with the Ni−O−C bond angle being similar to those of other nickel η^1-acetate complexes.

Electrochemical Studies. Representative cyclic voltammograms for complexes $[Ni(P^{Ph}{}_2N^{PhOMe}{}_2)_2(CH_3CN)]^{2+}$, $[Ni(P^{Cy}{}_2N^{Ph}{}_2)_2(CH_3CN)]^{2+}$, and $[Ni(P^{Cy}{}_2N^{Ph}{}_2)(P^{Ph}{}_2N^{Ph}{}_2)(CH_3CN)]^{2+}$ in acetonitrile solutions are shown in Figure 3 by traces a, b, and c, respectively. They consist of two reversible one-electron waves assigned to the Ni(II/I) and Ni(I/0) couples. This behavior is consistent with previous studies of $[Ni(diphosphine)_2]^{2+}$ complexes, and the potentials for these couples are listed in Table 1, together with related values from the literature. It can be seen from Figure 3 and Table 1 that the potentials of the Ni(II/I) couple are particularly sensitive to the nature of the substituents on phosphorus, shifting to more positive potentials as the number of cyclohexyl substituents increases.[12,22−24] This positive shift is somewhat counter-intuitive, in that replacing phenyl substituents on phosphorus with more electron-donating cyclohexyl groups would be expected to shift the potentials more negative on the basis of simple inductive effects. However, the increased steric bulk of the cyclohexyl substituents produces larger distortions toward tetrahedral geometry that lead to a lower energy for the lowest unoccupied molecular orbital (LUMO), as discussed elsewhere.[22−24] The lower energy of the LUMO results in a more positive potential for the Ni(II/I) couple.

Finally, it is of interest to compare the cyclic voltammogram of the hydride complex $[HNi(P^{Ph}{}_2N^{PhOMe}{}_2)_2]^+$ (Figure 4) to that of $[Ni(P^{Ph}{}_2N^{PhOMe}{}_2)_2(CH_3CN)]^{2+}$ (Figure 3a). Scanning anodically, $[HNi(P^{Ph}{}_2N^{PhOMe}{}_2)_2]^+$ shows a well-defined irreversible $2e^-$ oxidation at −0.47 V. The return cathodic scan shows reduction waves that correspond to the Ni(II/I) and Ni(I/0) couples of $[Ni(P^{Ph}{}_2N^{PhOMe}{}_2)_2(CH_3CN)]^{2+}$. This result suggests that the oxidation of $[HNi(P^{Ph}{}_2N^{PhOMe}{}_2)_2]^+$ is followed by rapid proton loss and a second electron transfer to generate $[Ni(P^{Ph}{}_2N^{PhOMe}{}_2)_2(CH_3CN)]^{2+}$, which is reduced on the return scan. At variable scan rates of 50 mV/s to 20 V/s, the wave at −0.47 V is irreversible, suggesting that proton transfer to the pendant amine following this oxidation is fast ($k > 50\ s^{-1}$). Similar behavior is observed for $[HNi(depe)_2](BF_4)$ (depe = 1,2-bis(diethylphosphino)ethane), but in that case the irreversible oxidation occurs at 0.0 V (the oxidation is irreversible at all observed scan rates, up to 100 V/s). This result suggests that the presence of a pendant base in $[HNi(P^{Ph}{}_2N^{PhOMe}{}_2)_2]^+$ results in a 0.5 V negative shift in potential. This potential shift is attributed to the pendant base assisting proton transfer upon oxidation of $[HNi(P^{Ph}{}_2N^{PhOMe}{}_2)_2]^+$, as previously observed for other

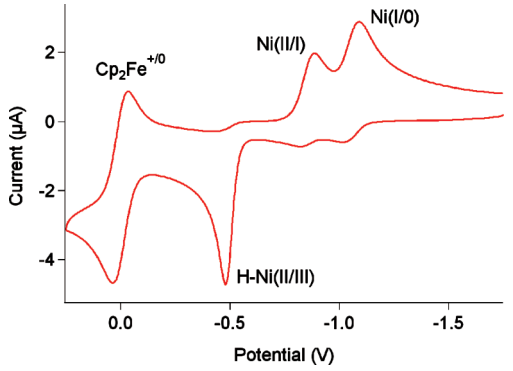

Figure 4. Cyclic voltammograms of $[HNi(P^{Ph}{}_2N^{PhOMe}{}_2)_2]^+$. Conditions: 1.6 mM complex in acetonitrile, 0.2 M NBu_4OTf as supporting electrolyte, glassy carbon working electrode, scan rate of 100 mV/s, with ferrocene as the internal reference at 0.0 V.

Table 1. Thermodynamic and Electrochemical Data in Acetonitrile and Benzonitrile

$NiL_2(CH_3CN)^{2+}$ ligands	$\Delta G°_{H^-}$ (kcal/mol)	$E_{1/2}(Ni^{II/I})$ (V vs $Cp_2Fe^{+/0}$)	$E(Ni^{I/0})$ (V vs $Cp_2Fe^{+/0}$)	pK_a of $HNiL_2^+$
$P^{Cy}_2N^{Ph}_2$	63.7	−0.62 (−0.60) [a]	−1.09 (−1.10) [a]	17.3
$P^{Cy}_2N^{Ph}_2$, $P^{Ph}_2N^{Ph}_2$	60.5	−0.76 (−0.76) [a]	−1.05 (−1.07) [a]	16.5
$P^{Ph}_2N^{PhOMe}_2$	58.6	−0.87 (−0.87) [a]	−1.07 (−1.08) [a]	17.4
$P^{Ph}_2N^{Ph}_2$ [c]	59.0	−0.84	−1.02	16.3
$P^{Ph}_2N^{PhCF3}_2$ [d]	61.4 [f]	−0.74	−0.89	13.8 [b]
$P^{Ph}_2N^{Bn}_2$	57.1	−0.94	−1.19	19.4
$P^{Ph}_2N^{Me}_2$ [e]	56.4 [f]	−0.98	−1.14	18.5 [b]
$P^{Cy}_2N^{Bn}_2$ [c]	60.7	−0.80	−1.28	21.2
$P^{Ph}_2N^{Bn}_2$, dppp [g]	68.4	(−0.52) [a]	(−1.04) [a]	18.0
dppp [h]		−0.12	−0.91	
depe [h]	56.0	−1.16 (−1.13) [a]	−1.29 (−1.30) [a]	23.8
dmpp [h]	62.1	−0.89 (−0.86) [a]	−1.33 (−1.32) [a]	23.9

[a] Values in parentheses are in benzonitrile. [b] Estimated from Ni(I/0) couple using pK_a = −18.6 $E_{1/2}$ = −2.65; see Figure 6. [c] Fraze et al.[9] [d] Kilgore et al.[16] [e] Yang et al.[28] [f] Estimated from Ni(II/I) couple using $\Delta G°_{H^-}$ = 20.8 $E_{1/2}$ + 76.8; see Figure 5. [g] Yang et al.[29] [h] dppp = 1,3-bis(diphenylphosphino)-propane, depe = 1,2-bis(diethylphosphino)ethane, dmpp = 1,2-bis(dimethylphosphino)propane. Berning et al.[30]

complexes containing diphosphine ligands with pendant amine bases.[25] It should be noted that the potentials for the nickel(II/I) and nickel(I/0) couples for $Ni(depe)_2^{2+}$ are actually an average of 0.25 V more negative than for $[Ni(P^{Ph}_2N^{PhOMe}_2)_2(CH_3CN)]^{2+}$, suggesting that the presence of the pendant amine may result in an even larger shift than suggested by simply the difference between the corresponding hydride oxidation potentials.

Thermodynamic Properties of Complexes $[HNi(P^{Ph}_2N^{PhOMe}_2)_2]^+$, $[HNi(P^{Cy}_2N^{Ph}_2)_2]^+$, and $[HNi(P^{Ph}_2N^{Ph}_2)(P^{Cy}_2N^{Ph}_2)]^+$. The hydride donor ability ($\Delta G°_{H^-}$) in acetonitrile for each of the three complexes was calculated from the observed equilibrium concentrations of the hydride with the starting complex using the thermodynamic cycle shown in Scheme 1.[26,27] The equilibrium between the hydride complex $[HNi(P^R_2N^{R'}_2)_2]^+$ and $[Ni(P^R_2N^{R'}_2)_2(CH_3CN)]^{2+}$ was measured by $^{31}P\{^1H\}$ and ^1H NMR spectroscopy using an appropriate base under 1.0 atm of hydrogen (eq 5). The sum of reactions 5−7 is reaction 8 (the heterolytic cleavage of the Ni−H bond to form H^- and the corresponding Ni(II) complex), and the free energy associated with this reaction is $\Delta G°_{H^-}$, the hydride donor ability. The reverse reaction corresponds to the hydride acceptor ability of $[Ni(P^R_2N^{R'}_2)_2(CH_3CN)]^{2+}$. Larger values of $\Delta G°_{H^-}$ correspond to better hydride acceptors and lower values to better hydride donors. This information is summarized in Table 1, together with data for selected additional complexes from the literature.

For the new complexes considered here, $[HNi(P^{Cy}_2N^{Ph}_2)_2]^+$ is the poorest hydride donor, with $\Delta G°_{H^-}$ = 63.7 kcal/mol, and $[HNi(P^{Ph}_2N^{PhOMe}_2)_2]^+$ is the best hydride donor, with $\Delta G°_{H^-}$ = 58.6 kcal/mol. The hydride donor ability for the heteroleptic complex $[HNi(P^{Cy}_2N^{Ph}_2)(P^{Ph}_2N^{Ph}_2)(CH_3CN)]^+$, 60.5 kcal/mol, is only slightly poorer than the hydride donor ability of the homoleptic complex $[HNiP^{Ph}_2N^{Ph}_2)_2]^+$, 59.0 kcal/mol. The p$K_a$ values for the $[HNi(P^R_2N^{R'}_2)_2]^+$ complexes were determined through thermochemical cycles using the hydride donor abilities and the electrochemical potentials for the Ni(II/I) and Ni(I/0) couples in acetonitrile, as previously reported for similar complexes.[31] The hydride donor abilities of the nickel complexes show the expected linear trend with the Ni(II/I) couple, and the pK_a values for the metal hydrides also exhibit a linear trend with the Ni(I/0) couple, as shown in Figures 5 and 6. These trends are very similar to the trends previously observed for nickel bis-diphosphine complexes with no pendant bases.[30] The heteroleptic complex is not shown in Figures 5 and 6, but the data for this complex are consistent with the trends observed for the homoleptic complexes.

Reactivity toward H_2 and CO_2 using High Pressure NMR Spectroscopy. The three new bis-$P^R_2N^{R'}_2$ complexes $[Ni(P^{Ph}_2N^{PhOMe}_2)_2(CH_3CN)]^{2+}$, $[Ni(P^{Cy}_2N^{Ph}_2)_2(CH_3CN)]^{2+}$, and $[Ni(P^{Cy}_2N^{Ph}_2)(P^{Ph}_2N^{Ph}_2)(CH_3CN)]^{2+}$ did not demonstrate any catalytic activity for CO_2 reduction under high pressures of CO_2 and H_2. The complexes were dissolved in acetonitrile-d_3, and the solutions were placed in a high-pressure PEEK NMR tube.[32,33] No reaction could be observed after applying 21 atm of a 1:1 mixture of CO_2/H_2. Even the independently synthesized hydride complex $[HNi(P^{Ph}_2N^{PhOMe}_2)_2]^+$ did not react observably with 21 atm of carbon dioxide. For complex $[Ni(P^{Cy}_2N^{Ph}_2)_2(CH_3CN)]^{2+}$, the formation of a hydride species could be observed without the addition of an external base, but no evidence for formation of formate or formic acid could be observed via NMR spectroscopy. These results are consistent

Scheme 1. Determination of Hydride Donor Abilities for $[HNi(P^R_2N^{R'}_2)_2]^+$ Complexes

	$\Delta G°$ (kcal/mol)	
$[HNi(P^R_2N^{R'}_2)_2]^+ + HB^+ \rightleftharpoons H_2 + [Ni(P^R_2N^{R'}_2)_2(CH_3CN)]^{2+} + B$	$-RT \ln K_{eq}$	(5)
$B + H^+ \rightleftharpoons HB^+$	-1.364 pK_a	(6)
$H_2 \rightleftharpoons H^+ + H^-$	76.0	(7)
$[HNi(P^R_2N^{R'}_2)_2]^+ \rightleftharpoons [Ni(P^R_2N^{R'}_2)_2(CH_3CN)]^{2+} + H^-$	$\Delta G°_{H^-} = -RT \ln K_{eq}$ -1.364 pK_a +76.0	(8)

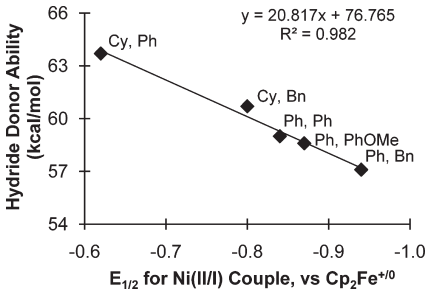

Figure 5. Correlation of the potential of the Ni(II/I) couple for $[Ni(P^{R}_2N^{R'}_2)_2(CH_3CN)]^{2+}$ complexes with the hydride donor ability for the corresponding hydrides. The designations for each point (R, R′) indicate phosphorus and nitrogen substituents, respectively.

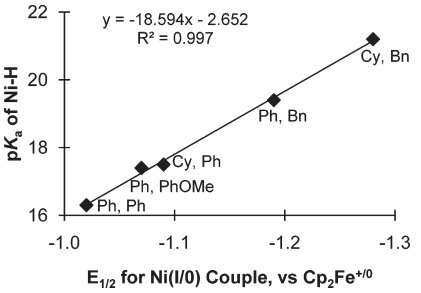

Figure 6. Correlation of the potential of the Ni(I/0) couple for $[Ni(P^{R}_2N^{R'}_2)_2(CH_3CN)]^{2+}$ complexes with the pK_a for the corresponding hydrides. The designations for each point (R, R′) indicate phosphorus and nitrogen substituents, respectively.

with thermodynamic data discussed in more detail below, wherein the transfer of a hydride to CO_2 to generate formate (ΔG_{H^-} = 44 ± 2 kcal/mol)[11] from a nickel hydride (ΔG_{H^-} = 56−64 kcal/mol in this study) is thermodynamically unfavorable.

Electrocatalytic Oxidation of Formate. The complexes $[Ni(P^{Ph}_2N^{PhOMe}_2)_2(CH_3CN)]^{2+}$, $[Ni(P^{Cy}_2N^{Ph}_2)_2(CH_3CN)]^{2+}$, and $[Ni(P^{Cy}_2N^{Ph}_2)(P^{Ph}_2N^{Ph}_2)(CH_3CN)]^{2+}$ were also examined for their activity for electrocatalytic formate oxidation. The left-hand side of Figure 7 shows cyclic voltammograms of $[Ni(P^{Cy}_2N^{Ph}_2)(P^{Ph}_2N^{Ph}_2)(CH_3CN)]^{2+}$ as a function of formate concentration (added as $NBu_4HCO_2\cdot HCO_2H$). The reversible wave at −1.33 V is due to the cobaltocenium/cobaltocene couple, used as an internal standard. This compound was used instead of ferrocene because the ferrocenium/ferrocene couple overlaps the catalytic waves observed for formate oxidation. The reversible wave at ∼−1.1 V is assigned to the Ni(I/0) couple as discussed above. The reversible nature of this wave as the concentration of formate increases implies that the Ni(I) and Ni(0) species do not react directly with formate. The wave at ∼−0.8 V is assigned to the Ni(II/I) couple. The latter wave has an increase in current with increasing formate concentration, shifts to more negative potentials, and assumes a shape more closely resembling a plateau rather than a diffusional peak shape. The negative shift in potential is consistent with a fast following reaction, likely the binding of formate following the oxidation of Ni(I) to form Ni(II). The increase in current upon oxidation of the complex to the Ni(II) oxidation state and the plateau-shaped wave are consistent with the electrocatalytic oxidation of formate.

The catalytic current enhancement (i_{cat}/i_p) observed in the presence of formate can be converted to a catalytic rate using eqs 9−12 (i_{cat} and i_p are the current in the presence and absence of substrate, respectively). Dividing eq 9 by eq 10 gives eq 11, wherein the terms for the area of the electrode (A), the diffusion coefficient (D), and the concentration of the catalyst are all eliminated. Equation 11 expresses i_{cat}/i_p in terms of the number of electrons in the catalytic process (n_{cat}), the universal gas constant (R), the temperature in Kelvin (T), Faraday's constant (F), the scan rate in V/s (υ), the number of electrons in the wave in the absence substrate (n_p), and the observed rate constant for the catalytic reaction (k).[34−36] A catalytic turnover frequency (TOF) can be calculated by converting eq 11 to eq 12 through a simple rearrangement. The results of the kinetic studies are summarized in Table 2, where the reported TOF is the highest TOF observed, as calculated using eq 12.

$$i_{cat} = n_{cat}FA[\text{catalyst}](Dk[HCO_2^-]^x)^{1/2} \quad (9)$$

$$i_p = 0.4463\left(\frac{F^3}{RT}\right)^{1/2} n_p^{3/2}AD^{1/2}[\text{catalyst}]\upsilon^{1/2} \quad (10)$$

$$\frac{i_{cat}}{i_p} = \frac{n_{cat}}{0.4463}\sqrt{\frac{RT}{F\upsilon {n_p}^3}}\sqrt{k[HCO_2^-]^x} \quad (11)$$

$$\text{TOF} = k[HCO_2^-]^x = \frac{F\upsilon {n_p}^3}{RT}\left(\frac{0.4463}{n_{cat}}\right)^2\left(\frac{i_{cat}}{i_p}\right)^2 \quad (12)$$

A plot of the TOF of the catalyst versus the concentration of formate (as $NBu_4HCO_2\cdot HCO_2H$) is shown on the right-hand side of Figure 7. It can be seen that the TOF initially increased linearly as a function of formate concentration, became independent of formate concentration between ∼0.04 and 0.06 M, and slowly decreased at higher formate concentrations. The initially linear region of this plot implies a first-order dependence of the TOF on formate concentration. The formate-independent region indicates a change in the rate-determining step from one that is first-order in formate to one that is independent of formate. The slow decrease above ∼0.08 M formate is likely due to catalyst decomposition. Loss of $P^{R}_2N^{R'}_2$ ligand from the nickel complex has been observed at high formate concentrations after hours in solution or in the presence of excess acetate, as indicated by the appearance of free $P^{R}_2N^{R'}_2$ ligand in the ^{31}P NMR spectrum.

The left-hand side of Figure 8 shows a series of cyclic voltammograms recorded in benzonitrile solutions of $[Ni(P^{Cy}_2N^{Ph}_2)(P^{Ph}_2N^{Ph}_2)(CH_3CN)]^{2+}$ as a function of catalyst concentration in the presence of excess formate (0.15 M $NBu_4HCO_2\cdot HCO_2H$). It can be seen that the catalytic current increases as the concentration of the catalyst increases. On the right-hand side of Figure 8 is a plot of the catalytic current (i_{cat}) as a function of the catalyst concentration obtained from the data on the left-hand side of the figure. The linear dependence of this plot on catalyst concentration implies that the catalytic reaction is first-order in catalyst. The data taken together implies that at low formate concentrations, the rate-determining step includes the reaction of formate with the catalyst, while at high formate concentrations the rate of reaction is still first-order in catalyst but appears to become independent of formate concentration. However, decay of the TOF at high formate concentration, likely

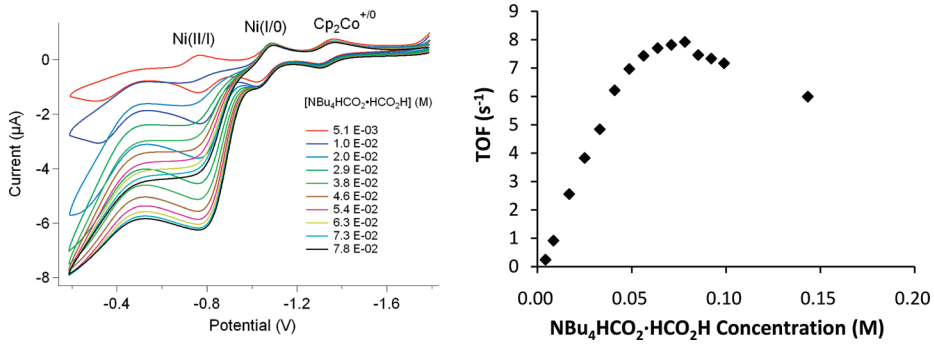

Figure 7. Left: CVs of the titration of $[Ni(P^{Cy}{}_2N^{Ph}{}_2)(P^{Ph}{}_2N^{Ph}{}_2)(CH_3CN)]^{2+}$, with $NBu_4HCO_2 \cdot HCO_2H$. Right: Corresponding turnover frequency versus $[NBu_4HCO_2 \cdot HCO_2H]$. Conditions: 1.2 mM catalyst solution in benzonitrile, 0.2 M NBu_4OTf as supporting electrolyte, glassy carbon working electrode, scan rate 50 mV/s. Potentials are referenced with respect to the ferrocenium/ferrocene couple (0.00 V) using the cobaltocenium/cobaltocene couple as a secondary reference (−1.33 V).

Table 2. Electrocatalytic TOFs and Thermochemical Data

$NiL_2(CH_3CN)^{2+}$ ligands	TOF (s^{-1})[a]	$\Delta G°_{H^-}$ (kcal/mol)[b]	pK_a of $HNiL_2{}^{+}$[b]	pK_a of free $R'NH_3{}^{+}$[b]
$P^{Ph}{}_2N^{Me}{}_2$[c]	15.8	56.4[g]	18.5[h]	18.37[i]
$P^{Ph}{}_2N^{Bn}{}_2$[d]	12.5	57.1	19.4	16.91[i]
$P^{Cy}{}_2N^{Bn}{}_2$[d]	9.6	60.7	21.2	16.91[i]
$P^{Ph}{}_2N^{PhOMe}{}_2$	8.7	58.6	17.4	11.86[j]
$P^{Cy}{}_2N^{Ph}{}_2$, $P^{Ph}{}_2N^{Ph}{}_2$	7.9	60.5	16.5	10.62[j]
$P^{Ph}{}_2N^{Ph}{}_2$[d]	7.4	59.0	16.3	10.62[j]
$P^{Ph}{}_2N^{PhCF3}{}_2$[e]	3.4	61.4[g]	13.8[h]	8.03[j]
$P^{Cy}{}_2N^{Ph}{}_2$	<1.1	63.7	17.3	10.62[j]
depe[f]	<0.4	56.0	23.8	–

[a] Data collected in benzonitrile with ∼1 mM complex and 0.2 M NBu_4OTf, where value shown is the maximum observed TOF. [b] Thermochemical values in acetonitrile. [c] Yang et al.[28] [d] Fraze et al.[9] [e] Kilgore et al.[16] [f] depe = 1,2-bis(diethylphosphino)ethane. Berning et al.[30] [g] Estimated from Ni(II/I) couple using $\Delta G°_{H^-} = 20.8\ E_{1/2} + 76.8$; see Figure 5. [h] Estimated from Ni(I/0) couple using p$K_a = -18.6\ E_{1/2} = -2.65$; see Figure 6. [i] Izutsu.[37] [j] Kaljurand et al.[38]

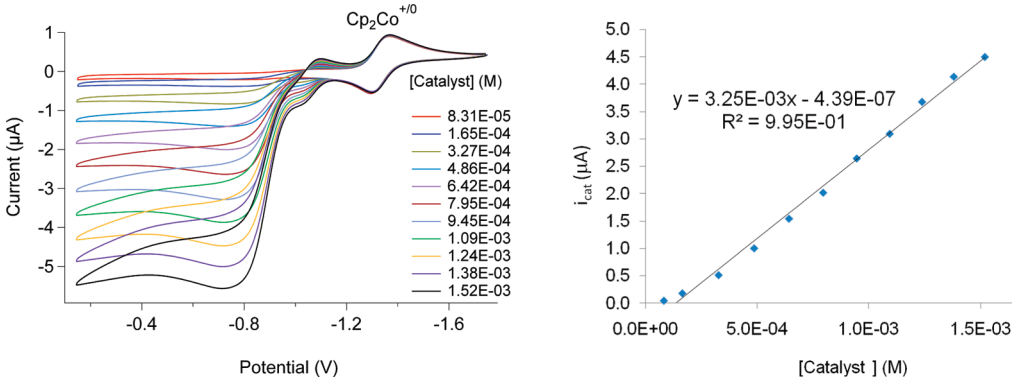

Figure 8. Left: CVs of the titration of $NBu_4HCO_2 \cdot HCO_2H$ with $[Ni(P^{Cy}{}_2N^{Ph}{}_2)(P^{Ph}{}_2N^{Ph}{}_2)(CH_3CN)]^{2+}$. Right: i_{cat} vs the concentration of $[Ni(P^{Cy}{}_2N^{Ph}{}_2)(P^{Ph}{}_2N^{Ph}{}_2)(CH_3CN)]^{2+}$. Conditions: 0.15 M $NBu_4HCO_2 \cdot HCO_2H$ solution in benzonitrile, 0.2 M NBu_4OTf as supporting electrolyte, glassy carbon electrode, scan rate 50 mV/s. Potentials are referenced with respect to the ferrocenium/ferrocene couple using cobaltocenium as a secondary internal reference.

a result of catalyst decomposition, complicates the interpretation of the formate concentration-independent region.

Due to $NBu_4HCO_2 \cdot HCO_2H$ being a simple, soluble, crystalline solid, this was used as the formate source throughout the present studies. This soluble salt does contain a co-crystallized formic acid that is homoconjugated with the formate; however, the formic acid was not expected to have a substantial effect on catalysis. In order to evaluate the effect of the formic acid, the electrocatalytic formate oxidation was repeated for $[Ni(P^{Ph}{}_2N^{PhOMe}{}_2)_2(CH_3CN)]^{2+}$ with a solution containing $NBu_4HCO_2 \cdot HCO_2H$ with an equimolar amount of DBU to deprotonate the formic acid and thereby generate formate and

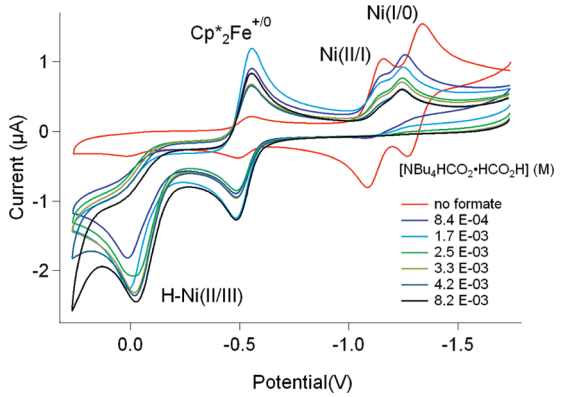

Figure 9. Cyclic voltammograms for the titration of $[Ni(depe)_2]^{2+}$ with $NBu_4HCO_2 \cdot HCO_2H$. Conditions: 0.98 mM $[Ni(depe)_2]^{2+}$ in benzonitrile, 0.2 M NBu_4OTf as supporting electrolyte, glassy carbon working electrode, scan rate 50 mV/s. Potentials are referenced with respect to the ferrocenium/ferrocene couple using permethylferrocene as a secondary internal standard.

protonated DBU. The result of using 1 equiv of DBU per $NBu_4HCO_2 \cdot HCO_2H$ was a very similar overall catalytic TOF of 10.6 s^{-1} with DBU vs 8.5 s^{-1} using $NBu_4HCO_2 \cdot HCO_2H$ without DBU (see Experimental Section for additional details).

To determine that CO_2 was indeed the product of the catalytic reaction, a controlled potential electrolysis was carried out using $[Ni(P^{Ph}{}_2N^{PhOMe}{}_2)_2(CH_3CN)]^{2+}$ as the catalyst (0.76 mM) in an acetonitrile solution containing 0.086 M $NBu_4HCO_2 \cdot HCO_2H$ at a potential ~100 mV positive of the peak of the catalytic current. After passing 16.3 C of charge (~8 turnovers), the headspace was analyzed by gas chromatography, and CO_2 but no H_2 was observed. Quantification of the CO_2 indicated a current efficiency of 93 ± 5% for this reaction. The protons were presumably trapped by formate to produce formic acid.

For comparison, the complex $[Ni(depe)_2]^{2+}$ was also studied to determine if a similar complex without a pendant amine would be a catalyst for formate oxidation. As seen in Figure 9, addition of increasing amounts of $NBu_4HCO_2 \cdot HCO_2H$ to acetonitrile solutions of $[Ni(depe)_2]^{2+}$ results in the formation of $[HNi(depe)_2]^{+}$, which shows a $2e^-$ oxidation at ~0 V vs $Cp_2Fe^{+/0}$ ($Cp^*{}_2Fe^{+/0}$ used as the internal reference). The lack of current enhancement beyond the $2e^-$ process at this $[HNi(depe)_2]^{+}$ oxidation indicates no measurable catalytic activity (<0.4 s^{-1}). This result indicates that the pendant amines play an important role in the observed catalytic activity of $Ni(P^R{}_2N^{R'}{}_2)_2{}^{2+}$ complexes.

DISCUSSION

The development of inexpensive and energy-efficient electrocatalysts for formate oxidation is essential for the utilization of formic acid fuel cells (the anodic half-reaction involved is shown in eq 13). In this reaction, formic acid is oxidized by two electrons, with the release of CO_2 and two protons. As with other multi-electron and multi-proton processes, the management of proton movement for catalysts of this type is of paramount importance. In previous work it has been demonstrated that pendant bases incorporated in the second coordination sphere of first-row transition metal complexes can serve as proton relays for catalytic oxidation and production of H_2 and for O_2 reduction.[10,17] In addition, the hydride donor abilities of $[HNi(diphosphine)_2]^{+}$ complexes are known to be in the range of 57−67 kcal/mol,[30] and the hydride donor ability of formate anion in acetonitrile is 44 ± 2 kcal/mol.[11] These data indicated that the formate anion should readily transfer a hydride to nickel to form CO_2 and a nickel hydride, and that these hydrides are the same intermediates involved in the oxidation of H_2 by $[Ni(P^R{}_2N^{R'}{}_2)_2(CH_3CN)]^{2+}$ complexes. As a result, it was anticipated that these complexes would be catalysts for formate oxidation.

$$HCO_2H \rightarrow CO_2 + 2H^+ + 2e^- \qquad (13)$$

A series of $[Ni(P^R{}_2N^{R'}{}_2)_2(CH_3CN)]^{2+}$ complexes were synthesized, characterized, and tested for electrocatalytic oxidation of formate. Systematic variation of the substituents at phosphorus and nitrogen allowed control over the hydride donor abilities and pK_a values for the corresponding nickel hydrides, which correlate with the reduction potentials for the Ni(II/I) and Ni(I/0) couples, respectively (as shown in Figures 5 and 6). These correlations provide estimates of the hydride donor abilities and pK_a values of the nickel hydrides from simple electrochemical potentials, which are more easily measured. The observed correlation is similar to the one previously reported for nickel bis-diphosphine complexes lacking a pendant base.[30]

Our initial expectation was that the catalytic rates of formate oxidation would parallel the hydride acceptor ability of the nickel catalyst, where in this series $[Ni(P^{Cy}{}_2N^{Ph}{}_2)_2(CH_3CN)]^{2+}$ is the best hydride acceptor and $[Ni(P^{Ph}{}_2N^{PhOMe}{}_2)_2(CH_3CN)]^{2+}$ is the worst. To test this hypothesis, we carried out a series of kinetic studies that showed that the TOF for each catalyst was dependent on formate concentrations below ~0.04 M (34 equiv $NBu_4HCO_2 \cdot HCO_2H$) and that above this concentration the TOF became formate concentration independent. In addition, the onset of the catalytic current was observed near the Ni(II/I) couple, consistent with no reaction of nickel(0) or nickel(I) with formate, followed by immediate reaction after oxidation to nickel(II). This interpretation is supported by NMR spectroscopic studies that demonstrate the nickel(II) complexes $[Ni(P^{Ph}{}_2N^{PhOMe}{}_2)_2(CH_3CN)]^{2+}$, $[Ni(P^{Cy}{}_2N^{Ph}{}_2)_2(CH_3CN)]^{2+}$, $[Ni(P^{Cy}{}_2N^{Ph}{}_2)(P^{Ph}{}_2N^{Ph}{}_2)(CH_3CN)]^{2+}$, and $[Ni(P^{Cy}{}_2N^{Bn}{}_2)_2]^{2+}$ all react with formate to form the corresponding hydride complexes. However, the concentration range over which the catalytic rates are dependent on formate concentration is small. At concentrations above ~0.06 M formate (52 equiv of $NBu_4HCO_2 \cdot HCO_2H$), where catalysis is most likely to be performed under practical conditions, the catalytic rate appears to become independent of formate concentration.

For the pendant base-containing complexes tested, $[Ni(P^{Cy}{}_2N^{Ph}{}_2)_2(CH_3CN)]^{2+}$ is the best hydride acceptor and yet the least active catalyst. In fact, the catalytic rates correlate poorly with the hydride acceptor abilities of these complexes, as shown in Table 2. The failure of the catalytic rate to correlate with the hydride acceptor ability is inconsistent with a rate-determining step involving direct hydride transfer from formate to the nickel center. The observation that $[Ni(depe)_2]^{2+}$ shows no observable catalytic activity in the presence of excess formate (as shown in Figure 9) indicates that the presence of the pendant amine is essential for catalysis.

To probe the binding of formate with the nickel center, $[Ni(P^{Ph}{}_2N^{Bn}{}_2)_2(CH_3CN)]^{2+}$ was synthesized as previously reported[9] and reacted with acetate to isolate a five-coordinate

Scheme 2. Proposed Reaction Scheme for Electrocatalytic Formate Oxidation

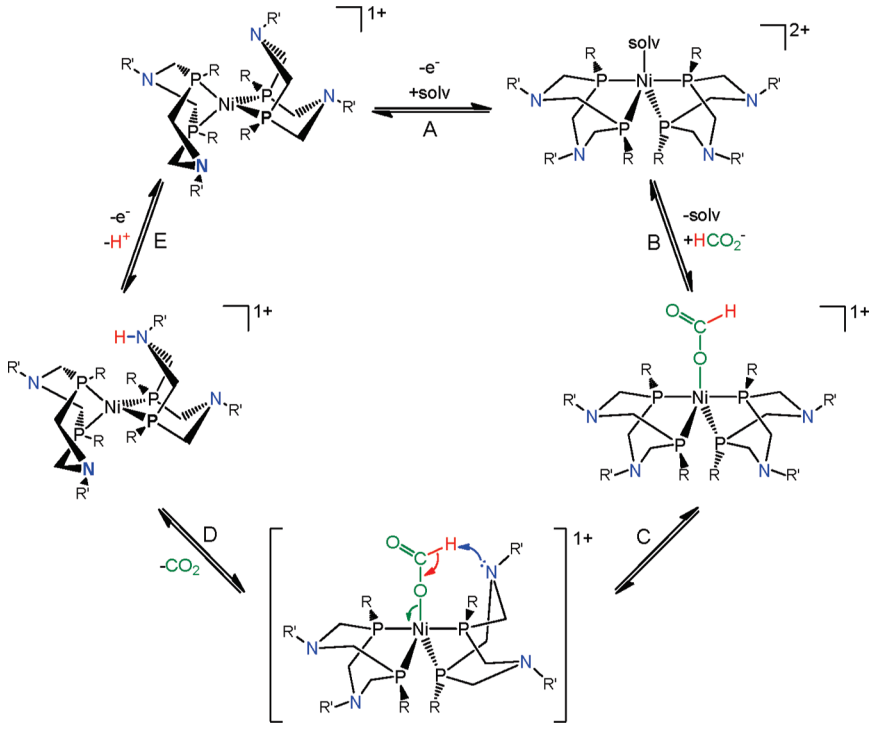

nickel acetate complex. The nickel acetate complex is stable, whereas the formate complex is not. This instability of the formate complex is attributed to the possible net hydride transfer to liberate CO_2 and generate the nickel hydride. Higher concentrations of acetate led to almost complete displacement of the phosphine ligands from nickel. This favorable binding of acetate suggests that formate may also bind through oxygen to form a complex analogous to the structurally characterized acetate complex, $[Ni(P^{Ph}{}_2N^{Bn}{}_2)_2(OAc)]^+$ (Figure 2), as shown in step B of the proposed catalytic cycle shown in Scheme 2.

For catalysts with a phenyl substituent at phosphorus, the catalytic activity correlates with the pK_a of the conjugate acid ($R'NH_3^+$) of the free amine used to make the corresponding $P^R{}_2N^{R'}{}_2$ ligand (see the blue data and line in Figure 10). This correlation and the lack of catalytic activity for $Ni(depe)_2^{2+}$ suggest that the rate-determining step requires the presence of the pendant amine. In addition, the homoleptic complexes with the bulkier cyclohexyl substituents at phosphorus exhibit lower TOFs than their phenyl analogues, indicating that increased steric bulk decreases catalytic activity. A mechanism that is consistent with all of the above observations is shown in Scheme 2. In this scheme, the oxidation of Ni(I) to Ni(II) is followed by a fast reaction with formate to generate $[Ni(P^R{}_2N^{R'}{}_2)_2(O_2CH)]^+$, with formate binding through one oxygen. The steric retardation of the catalytic rate for cyclohexyl vs phenyl substituents at phosphorus may be the result of this equilibrium step being shifted to disfavor formate association. As illustrated in steps C and D of Scheme 2, the oxygen-bound formate complex is thought to undergo a proton transfer from the carbon atom of formate to a pendant nitrogen atom with a concomitant transfer of two electrons to nickel and the release of CO_2. It is this heterolytic cleavage of formate that is proposed as the rate-limiting step in the overall catalytic cycle. Subsequent deprotonation and re-oxidation

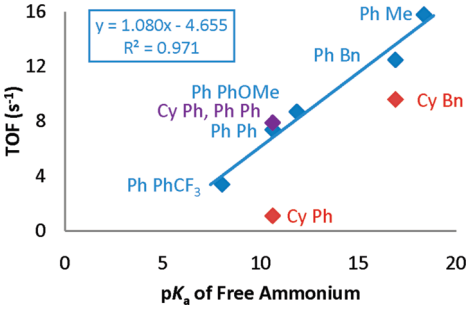

Figure 10. Correlation of TOF for electrocatalytic formate oxidation with the pK_a of the free primary ammonium ($R'NH_3^+$) used to synthesize the corresponding $P^R{}_2N^{R'}{}_2$ ligands for each $Ni(P^R{}_2N^{R'}{}_2)_2(CH_3CN)]^{2+}$ complex. The data point labels in the figure refer to the R and R′ substituents, respectively, and the trend line and corresponding equation are only for R = Ph.

of the resulting nitrogen protonated Ni(0) complex appears to be fast and leads to the reformation of Ni(I), as in step E of Scheme 2.

Regardless of the precise mechanistic features, which are still under investigation, a comparison of the TOFs observed for formate oxidation by the nickel-based catalysts used in this study with those of catalytic thermal formate oxidations show that the rates observed here (from <1 to 16 s^{-1}) at room temperature are comparable to those of the best molecular catalysts for formate oxidation reported to date in the literature: ruthenium complexes with TOFs of 3600 h^{-1} (1 s^{-1}) at 40 °C and 18 000 h^{-1} (5 s^{-1}) at 120 °C,[7,39,40] and iridium complexes with TOFs as high as 14 000 h^{-1} (4 s^{-1}) at 90 °C.[41,42] In addition, the failure to observe any measurable catalytic currents for analogous nickel diphosphine complexes lacking pendant amines illustrates the importance

dx.doi.org/10.1021/ja204489e |J. Am. Chem. Soc. 2011, 133, 12767–12779

of the pendant amines in catalytic reactions involving multi-electron and multi-proton processes.

SUMMARY AND CONCLUSIONS

Thermodynamic considerations of the hydride donor abilities of the formate ion and the hydride acceptor abilities of $[Ni(diphosphine)_2]^{2+}$ complexes suggested that hydride transfer from formate to these nickel complexes should occur. In addition, pendant amines were incorporated in the diphosphine ligands to assist in proton transfer reactions that were expected to occur during the catalytic reactions. Using these guidelines, new $[Ni(P^R_2N^{R'}_2)_2(CH_3CN)]^{2+}$ and previously reported complexes were prepared that allowed a systematic variation in the hydride acceptor ability of the metal and the basicity of the pendant amine. These $[Ni(P^R_2N^{R'}_2)_2(CH_3CN)]^{2+}$ complexes were demonstrated to be catalysts for the electrocatalytic oxidation of formate, and mechanistic studies demonstrated that the pendant amine plays an important role in the rate-determining step that is thought to involve proton transfer from the formate carbon atom to a pendant amine of the ligand. The catalytic TOFs for these electrocatalysts are as high as any reported thermal formate/formic acid oxidation catalysts, and to our knowledge, the present catalysts are the first electrocatalysts to utilize a base metal, nickel, rather than the more typical platinum, palladium, or rhodium. Furthermore, these are the first homogeneous complexes reported for the electrocatalytic oxidation of formate.

EXPERIMENTAL SECTION

Materials and Methods. All chemicals were purchased from commercial sources and used as received unless otherwise specified. The complexes $[Ni(P^{Cy}_2N^{Bn}_2)_2](BF_4)_2$, $[Ni(P^{Ph}_2N^{Ph}_2)_2(CH_3CN)](BF_4)_2$, $[Ni(P^{Ph}_2N^{Bn}_2)_2(CH_3CN)](BF_4)_2$, $[Ni(P^{Ph}_2N^{Me}_2)_2(CH_3CN)](BF_4)_2$, and $[Ni(P^{Ph}_2N^{PhCF3}_2)_2(CH_3CN)](BF_4)_2$ were prepared as previously described.[9,12,16,28] All manipulations were carried out using standard Schlenk and glovebox techniques under an atmosphere of nitrogen. Acetonitrile and tetrahydrofuran (THF) were sparged with argon and dried over basic alumina with a custom dry solvent system. Pentane and diethyl ether (Et_2O) were distilled over sodium benzophenone ketyl. ^1H, ^{13}C, and ^{31}P NMR spectra were recorded on a Varian 300, 400, or 500 spectrometer or a Jeol ECA-500 spectrometer. The ^1H and ^{13}C NMR spectra are referenced to TMS using the residual resonances of the solvent. The ^{31}P NMR shifts are referenced to H_3PO_4.

All electrochemical experiments were carried out under an atmosphere of nitrogen in a 0.2 M tetrabutylammonium trifluoromethanesulfonate (NBu_4OTf) solution in benzonitrile using a CH Instruments 600 or 1100 series three-electrode potentiostat. The working electrode was a glassy carbon disk (1 mm diameter), and the counter electrode was a glassy carbon rod. A silver wire in electrolyte solution separated from the working compartment by porous Vycor (4 mm, BAS) was used as a pseudo-reference electrode. All potentials were measured using Cp_2Fe (0 V), Cp^*_2Fe (−0.50 V), or Cp_2Co^+ (−1.33 V) as an internal reference, with all of the potentials reported vs the $Cp_2Fe^{+/0}$ couple. All stock solutions of catalyst, $NBu_4HCO_2 \cdot HCO_2H$, and electrolyte were freshly prepared in a glovebox under a nitrogen atmosphere. UV−vis spectra were collected on a Shimadzu UV-3600 instrument in 0.1 cm quartz cuvettes. IR spectra were recorded as KBr pellets using a FT-IR Bruker Equinox 55 spectrometer. Elemental analyses were performed by Midwest MicroLab, LLC, Indianapolis, IN, or by Atlantic Microlab, Inc., Norcross, GA.

Crystals of $[Ni(P^{Ph}_2N^{PhOMe}_2)_2(CH_3CN)](BF_4)_2$, $[Ni(P^{Cy}_2N^{Ph}_2)_2(CH_3CN)](BF_4)_2$, $[Ni(P^{Cy}_2N^{Ph}_2)(CH_3CN)_2](BF_4)_2$, $[Ni(P^{Cy}_2N^{Ph}_2)(P^{Ph}_2N^{Ph}_2)(CH_3CN)](BF_4)_2$, and $[Ni(P^{Ph}_2N^{PhOMe}_2)_2]$ suitable for X-ray structural determinations were mounted in polybutene oil on a glass fiber and transferred on the goniometer head to the precooled instrument. Crystallographic measurements were carried out on either a Bruker P4 or platform diffractometer using Mo Kα radiation (λ = 0.71073 Å) in conjunction with a Bruker APEX detector. All structures were solved by direct methods using SHELXS-97 and refined with full-matrix least-squares procedures using SHELXL-97.[43] All non-hydrogen atoms are anisotropically refined unless otherwise reported; the hydrogen atoms were included in calculated positions as riding models in the refinement. Crystallographic data collection and refinement information can be found in the Supporting Information.

X-ray Structural Analysis for $[Ni(P^{Ph}_2N^{Bn}_2)_2(OAc)](BF_4)$. A single red block (0.10 × 0.10 × 0.10 mm) was mounted using NVH immersion oil onto a nylon fiber and cooled to the data collection temperature of 100(2) K. Data were collected on a Brüker-AXS Kappa APEX II CCD diffractometer with 0.71073 Å Mo Kα radiation. Unit cell parameters were obtained from 36 data frames, 0.5° Φ, from three different sections of the Ewald sphere yielding a = 24.0216(11), b = 17.6157(8), and c = 17.6157(8) Å, V = 6180.8(5) Å^3. A total of 91 964 reflections (R_{int} = 0.1006) were collected (12 749 unique) over θ = 1.43−26.49°. The systematic absences in the diffraction data were consistent with the centrosymmetric, orthorhombic space group, *Pna*2(1). The data set was treated with SADABS absorption corrections based on redundant multiscan data (G. Sheldrick, Bruker-AXS, 2001), T_{max}/T_{min} = 1.00. The asymmetric unit contains one $[Ni(P^{Ph}_2N^{Bn}_2)_2(OAc)]^+$ cation, one $[BF_4]^-$ anion, and one molecule of Et_2O solvent located on general positions, yielding Z = 4 and Z' = 1. All non-hydrogen atoms were refined with anisotropic displacement parameters. All hydrogen atoms were treated as idealized contributions. The goodness-of-fit on F^2 was 1.022, with R1 ($wR2$) = 0.0429 (0.0889) for $[I\theta > 2(I)]$ and with largest difference peak and hole of 0.653 and −0.327 e/Å^3.

Synthesis of $[Ni(P^{Ph}_2N^{PhOMe}_2)_2(CH_3CN)](BF_4)_2$. Kilgore et al. very recently reported the synthesis of $[Ni(P^{Ph}_2N^{PhOMe}_2)_2(CH_3CN)](BF_4)_2$ using a similar procedure.[16] For details of the synthesis used for the present work, see the Supporting Information. Single crystals suitable for X-ray diffraction were obtained after several days by layering a concentrated acetonitrile solution with diethyl ether at −35 °C. ^1H and ^{31}P NMR data matched the previously reported data.[16] $^{13}C\{^1H\}$ NMR (CD_3CN, 20 °C, 125 MHz) δ [ppm]: 156.3 ($C_{arom}O$), 145.6 ($C_{arom}N$), 131.3 and 131.9 ($C_{arom}H$, P^{Ph}), 129.6 ($C_{arom}P$), 114.9 and 122.1 ($C_{arom}H$, N^{Ph}), 59.1 (PCH_2N), 55.5 (OCH_3). IR (KBr) ν_{max} [cm^{-1}]: 3057 (w), 3005 (w), 2938, (w), 2839 (w), 1511 (vs), 1438 (m), 1249 (s), 1191 (m), 1058 (s), 1035 (s), 890 (m), 839 (m), 816(w), 743 (m), 695 (m), 496 (m). Elemental analysis: C/H/N calcd for $NiC_{62}H_{67}N_5O_4P_4B_2F_8$, 57.18/5.19/5.38; found, 57.16/5.32/5.61.

Synthesis of $[Ni(P^{Cy}_2N^{Ph}_2)(CH_3CN)_2](BF_4)_2$. Cyclohexylphosphine (1.06 mL, 8 mmol) was placed in a Schlenk flask and was transferred with dry ethanol (150 mL) into another flask containing paraformaldehyde (0.46 g, 15 mmol). The reaction mixture was stirred under reflux for 2 h until the suspension became a clear solution. Aniline (0.73 mL, 8 mmol) dissolved in ethanol (20 mL) was added via cannula to the reaction flask, and the reaction mixture was stirred for 2 h under reflux. After 5 min the precipitation of a white fluffy solid was observed. The reaction was cooled to room temperature, the solvent removed by cannula filtration, and the precipitate washed twice with ethanol. The resulting white solid was dried in vacuum and used without further purification. Based on the initial cyclohexylphosphine, 0.8 equiv of $[Ni(CH_3CN)_6](BF_4)_2$ (1.08 g, 3.2 mmol) in acetonitrile was added to the crude ligand. The solution turned red and was stirred overnight. The resulting solution was filtered and layered with diethyl ether. After 2 days, large red needles of $[Ni(P^{Cy}_2N^{Ph}_2)(CH_3CN)_2](BF_4)_2$ were collected; yield, 59% (1.49 g, 1.9 mmol). Single crystals suitable for X-ray diffraction were obtained from a CH_3CN/Et_2O solution at −35 °C. ^1H NMR (CD_3CN, 20 °C, 400 MHz) δ [ppm]: 7.51 (t, 4H, ^3J = 8 Hz,

C_{arom}**H**, N^{Ph}), 7.21 (d, 4H, ^3J = 8 Hz, C_{arom}**H**, N^{Ph}), 7.16 (t, 2H, ^3J = 8 Hz, C_{arom}**H**, N^{Ph}), 4.02 (d, 4H, ^2J = 12 Hz, $P^{Cy}C\mathbf{H}_2N^{Ph}$), 3.58 (d, 4H, ^2J = 12 Hz, $P^{Cy}C\mathbf{H}_2N^{Ph}$), 2.41 (m broad, 2H, P^{Cy}), 2.03 (s broad, 4H, P^{Cy}), 1.85 (m broad, 4H, P^{Cy}), 1.76 (d, 2H, ^3J = 8 Hz, P^{Cy}), 1.52−1.41 (m, 8H, P^{Cy}), 1.36−1.31 (m broad, 2H, P^{Cy}). $^{31}P\{^1H\}$ NMR (CD_3CN, 20 °C, 162 MHz) δ [ppm]: 9.8 (s).

Synthesis of [Ni($P^{Cy}_2N^{Ph}_2$)($P^{Ph}_2N^{Ph}_2$)(CH_3CN)](BF_4)$_2$. The $P^{Ph}_2N^{Ph}_2$ ligand[12] was prepared using the same procedure as for $P^{Cy}_2N^{Ph}_2$ described above, but with phenylphosphine (0.375 mL, 2.8 mmol), paraformaldehyde (168 mg, 5.6 mmol), and aniline (0.256 mL, 2.8 mmol) as reagents. After filtration and drying of the resulting white solid in vacuum, 0.8 equiv of [Ni($P^{Cy}_2N^{Ph}_2$)(CH_3CN)$_2$](BF_4)$_2$ (0.85 g, 1.1 mmol) was added to the crude ligand via cannula. The reaction mixture was stirred overnight, resulting in a dark red mixture. After filtration, the solvent was removed, and the dark red solid was dried under vacuum. The product was recrystallized by layering a concentrated acetonitrile solution with diethyl ether at room temperature. Single crystals suitable for X-ray diffraction were obtained by vapor diffusion of diethyl ether into a concentrated solution of [Ni($P^{Cy}_2N^{Ph}_2$)($P^{Ph}_2N^{Ph}_2$)(CH_3CN)](BF_4)$_2$ in acetonitrile at −35 °C; yield, 67% (0.90 g, 0.75 mmol). ^1H NMR (CD_3CN, 20 °C, 500 MHz) δ [ppm]: 7.85−7.82 (m, 2H, C_{arom}**H**, P^{Ph}), 7.72 (t, 1H, ^3J = 8 Hz, C_{arom}**H**, P^{Ph}), 7.61 (t, 1H, ^3J = 8 Hz, C_{arom}**H**, P^{Ph}), 7.40−7.34 (m, 4H, C_{arom}**H**, N^{Ph}), 7.25 (d, 2H, ^3J = 9 Hz, C_{arom}**H**, N^{Ph}), 7.13 (d, 2H, ^3J = 9 Hz, C_{arom}**H**, N^{Ph}), 7.08−7.04 (m, 2H, C_{arom}**H**, N^{Ph}) 4.50−3.65 (broad, 2H, $P^{Ph}C\mathbf{H}_2N^{Ph}$, 4H $P^{Cy}C\mathbf{H}_2N^{Ph}$), 3.61 (d, 2H, ^2J = 14 Hz, $P^{Ph}C\mathbf{H}_2N^{Ph}$), 1.60−1.44 (m broad, 5H, P^{Cy}), 1.32−1.19 (m broad, 2H, P^{Cy}), 1.11−1.04 (m, 1H, P^{Cy}), 0.92 (t broad, 1H, ^2J = 12 Hz, P^{Cy}), 0.86−0.38 (broad, 1H, P^{Cy}). $^{13}C\{^1H\}$ NMR (CD_3CN, 20 °C, 75.5 MHz) δ [ppm]: 152.5 and 152.3 ($\mathbf{C}_{arom}$N), 40.8 ($\mathbf{C}_{arom}$H, N^{Ph}), 133.8 (m, $\mathbf{C}_{arom}$, P^{Ph}), 132.8 ($\mathbf{C}_{arom}$H, N^{Ph}), 131.6 (m, $\mathbf{C}_{arom}$, P^{Ph}), 130.7 and 130.5 (broad, $\mathbf{C}_{arom}$, P^{Ph}), 124.1, 123.2, 120.7 and 119.4 ($\mathbf{C}_{arom}$H, N^{Ph}), 47.4 and 36.0 (broad, P$\mathbf{C}H_2$N), 28.5 and 27.8 (broad, P^{Cy}), 25.7 (P^{Cy}). $^{31}P\{^1H\}$ NMR (CD_3CN, 20 °C, 121 MHz) δ [ppm]: 8.40−7.40 (m) and 3.05−7.93 (m). IR (KBr) ν_{max} [cm^{-1}]: 3389 (w), 3083 (w), 2986 (w), 2884 (w), 2822 (w), 1581 (s), 1485 (s), 1430 (vs), 1268 (m), 1226 (s), 1176 (s), 1131 (s), 969 (m), 894 (m), 857 (m), 770 (m), 718 (m), 685 (m), 514 (m), 459 (w). Elemental analysis: C/H/N calcd for $NiC_{58}H_{71}N_5P_4B_2F_8$, 58.32/5.99/5.86; found, 58.08/6.11/5.73.

Synthesis of [Ni($P^{Cy}_2N^{Ph}_2$)$_2$(CH_3CN)](BF_4)$_2$. The ligand $P^{Cy}_2N^{Ph}_2$ was synthesized as described above for [Ni($P^{Cy}_2N^{Ph}_2$)(CH_3CN)$_2$]$^{2+}$. [Ni(CH_3CN)$_6$](BF_4)$_2$ (257 mg, 0.5 mmol) was dissolved in degassed acetonitrile (100 mL total) and transferred via cannula into a flask containing the crude ligand (0.49 g, 1.0 mmol). The reaction mixture immediately changed to red. After being stirred overnight, the reaction mixture was canula filtered to remove unreacted ligand, and the solvent was then removed by vacuum. The resulting red solid was recrystallized from an acetonitrile solution of [Ni($P^{Cy}_2N^{Ph}_2$)$_2$(CH_3CN)](BF_4)$_2$ layered with diethyl ether at room temperature. Single crystals suitable for X-ray diffraction were obtained from a concentrated acetonitrile diethyl ether solution of the compound at −35 °C; yield, 73% (453 mg, 375 μmol). ^1H NMR (CD_3CN, 20 °C, 400 MHz) δ [ppm]: 7.35 (t, 8H, ^3J = 8 Hz, C_{arom}**H**, N^{Ph}), 7.10−7.04 (m, 12H, C_{arom}**H**, N^{Ph}), 4.08 (d, 4H, ^2J = 16 Hz, P$\mathbf{C}H_2$N), 3.82−3.73 (m, 8H, P$\mathbf{C}H_2$N), 3.56 (d, 4H, 2J = 16 Hz, P$\mathbf{C}H_2$N), 2.24 (t, 6H, J = 12 Hz, P^{Cy}), 2.10 (d, 4H, J = 12 Hz, P^{Cy}), 1.91−1.32 (m, 34H, P^{Cy}). $^{13}C\{^1H\}$ NMR (CD_3CN, 20 °C, 300 MHz) δ [ppm]: 151.8 ($\mathbf{C}_{arom}$N, $^3J_{P-C}$ = 4 Hz), 130.4, 123.1, and 119.2 ($\mathbf{C}_{arom}$H), 49.3−49.1 and 47.4−47.1 (m broad, P$\mathbf{C}H_2$N), 39.7 (m, coord CH_3CN), 28.9 ($\mathbf{C}^{Cy}$P), 28.2 (broad, $\mathbf{C}^{Cy}$), 27.6 (broad, $\mathbf{C}^{Cy}$), 25.9 ($\mathbf{C}^{Cy}$); the signal for the quaternary carbon nucleus of the CH_3CN could not be detected. $^{31}P\{^1H\}$ NMR (CD_3CN, 20 °C, 162 MHz) δ [ppm]: 7.2 (s). IR (KBr) ν_{max} [cm^{-1}]: 3063 (w), 2958 (m), 2909 (m), 2849 (m), 1598 (m), 1496 (m), 1452 (w), 1272 (w), 1195(m) 1100 (s), 1021 (s), 890 (w), 759 (w), 695 (w), 521 (vs). Elemental analysis: C/H/N calcd for $NiC_{58}H_{83}N_5P_4B_2F_8$, 57.74/6.93/5.80; found, 57.88/6.92/6.11.

Synthesis of [HNi($P^{Ph}_2N^{PhOMe}_2$)$_2$](BF_4. **Method a:** [Ni($P^{Ph}_2N^{PhOMe}_2$)$_2$(CH_3CN)](BF_4)$_2$ (63.2 mg, 48.5 μmol) was dissolved in acetonitrile in a glovebox, and this solution was added to a vial containing excess sodium formate. The red solution turned yellow over 20 min. The excess sodium formate was removed by filtration, and the product was isolated by removing the solvent under vacuum. The resulting solid was washed twice with pentane and dried under vacuum. **Method b:** The hydride complex [HNi($P^{Ph}_2N^{PhOMe}_2$)$_2$](BF_4) can be obtained by the same procedure using [Ni($P^{Ph}_2N^{PhOMe}_2$)$_2$(CH_3CN)](BF_4)$_2$ (101.6 mg, 78 μmol) and 1 equiv of sodium trimethoxyborohydride ($NaB(OMe)_3H$) (10.0 mg, 78 μmol) instead of sodium formate. ^1H NMR (CD_3CN, 20 °C, 400 MHz) δ [ppm]: 7.62−7.61 (m, 8H, C_{arom}**H**, P^{Ph}), 7.46 (t, 4H, ^3J = 7.4 Hz, C_{arom}**H**, P^{Ph}), 7.26 (t, 8H, ^3J = 7.6 Hz, C_{arom}**H**, P^{Ph}), 7.03 (d, 8H, ^3J = 9.2 Hz, C_{arom}**H**, N^{Ph}), 6.89 (d, 8H, ^3J = 9.2 Hz, C_{arom}**H**, N^{Ph}), 3.89 (d, 8H, ^2J = 12.8 Hz, P$\mathbf{C}H_2$N), 3.78 (s, 12H, P$\mathbf{C}H_2$N), 3.42 (d, 8H, ^2J = 13.2 Hz, P$\mathbf{C}H_2$N), −8.05 (quintet, 1H, ^2J = 30.3 Hz, Ni-**H**). $^{31}P\{^1H\}$ NMR (CD_3CN, 20 °C, 162 MHz) δ [ppm]: 15.1 (s).

Synthesis of [Ni($P^{Ph}_2N^{PhOMe}_2$)$_2$. **Method a:** [Ni($P^{Ph}_2N^{PhOMe}_2$)$_2$(CH_3CN)](BF_4)$_2$ (63.2 mg, 48.5 μmol) was dissolved in acetonitrile and added to a vial containing excess sodium formate. The red solution turned yellow over 20 min, and a yellow precipitate formed. The reaction was complete when the solution became transparent, indicating complete precipitation of the product. The solvent was removed by filtration, and the resulting solid, a mixture of $NaBF_4$, $NaHCO_2$, and [Ni($P^{Ph}_2N^{PhOMe}_2$)$_2$], was dried under vacuum and washed three times with pentane. The product can be extracted with THF. Single crystals suitable for X-ray diffraction were obtained by vapor diffusion of pentane into a concentrated THF solution of [Ni($P^{Ph}_2N^{PhOMe}_2$)$_2$]. **Method b:** Complex [Ni($P^{Ph}_2N^{PhOMe}_2$)$_2$] was also obtained by the same procedure through the reaction of the complex [Ni($P^{Ph}_2N^{PhOMe}_2$)$_2$(CH_3CN)](BF_4)$_2$ (101.6 mg, 78 μmol) with 2 equiv of sodium trimethoxyborohydride ($NaB(OMe)_3H$) (20.0 mg, 156 μmol) instead of sodium formate. ^1H NMR (THF-d_8, 20 °C, 300 MHz) δ [ppm]: 7.86 (t, broad, 8H, J = 6 Hz, C_{arom}**H**, P^{Ph}), 7.01−7.10 (m, 12H, C_{arom}**H**, P^{Ph}), 6.99 (d, 8H, ^3J = 9 Hz, C_{arom}**H**, N^{Ph}), 6.77 (d, 8H, ^3J = 9 Hz, C_{arom}**H**, N^{Ph}), 3.89 (d, 8H, ^2J = 12 Hz, P$\mathbf{C}H_2$N), 3.70 (s, 12H), 3.50 (d, 8H, ^2J = 12 Hz, P$\mathbf{C}H_2$N), 3.45 (s, 12H). $^{31}P\{^1H\}$ NMR (THF-d_8, 20 °C, 121.5 MHz) δ [ppm]: 7.5 (s).

Synthesis of [Ni($P^{Ph}_2N^{Bn}_2$)$_2$(OAc)](BF_4)·Et_2O. A solution of tetrabutylammonium acetate (14.5 mg, 0.049 mmol) in benzonitrile was added to a solution of [Ni($P^{Ph}_2N^{Bn}_2$)$_2$(CH_3CN)](BF_4)$_2$ (60 mg, 0.048 mmol) in benzonitrile. The solution immediately changed from red to dark purple. Vapor diffusion of diethyl ether into the crude reaction mixture at room temperature afforded dark red crystals suitable for X-ray crystallography; yield, 38% (21 mg, 0.018 mmol). $^{31}P\{^1H\}$ NMR (CD_2Cl_2, 20 °C): an AA′BB′ spectrum was observed with resonances centered at 20.4 and −18.6 ppm.

Synthesis of NBu_4HCO_2·HCO_2H. A solution of tetrabutylammonium hydroxide (3.8 M, 5.0 mL, 19 mmol) was placed into a Schlenk flask with a stir bar. Formic acid (0.96 mL, 19.0 mmol) was added dropwise over 5 min at room temperature and allowed to stir for 3 h. Water (0.5 mL) was added to reaction mixture, which was then extracted with EtOAc (3 × 15 mL). The organic phase was dried over $MgSO_4$ and concentrated to give a colorless oil. Diethyl ether (30 mL) was added and concentrated again, yielding a tacky white solid. The solid was dried under vacuum for several hours and stored in a glovebox. The product was crystallized by layering a saturated solution of NBu_4HCO_2·HCO_2H in THF with hexane; yield, 1.96 g (6.8 mmol), 36%. ^1H NMR (300 MHz, CD_3CN) δ [ppm]: 18.7 (s, 0.8 H, HCO_2**H**-O_2CH), 8.55 (s, 1.7 H, **H**CO_2H-O_2C**H**), 3.22 (m,

dx.doi.org/10.1021/ja204489e |J. Am. Chem. Soc. 2011, 133, 12767–12779

8.4 H, $N(CH_2CH_2CH_2CH_3)_4$), 1.70 (m, 8.4 H, $N(CH_2CH_2CH_2CH_3)_4$), 1.43 (sextet, 8.2 H, J_{H-H} = 6.0 Hz, $N(CH_2CH_2CH_2CH_3)_4$), 1.04 (t, 12.0 H, J_{H-H} = 6.0 Hz, $N(CH_2CH_2CH_2CH_3)_4$). Elemental analysis: C/H/N calcd for $C_{18}H_{39}NO_4$, C, 64.82; H, 11.79; N, 4.20; found, C, 64.22; H, 11.53; N, 4.29.

General Procedure for Hydricity Determination by Heterolytic H_2 Cleavage: $[Ni(P^{Ph}_2N^{PhOMe}_2)_2(CH_3CN)](BF_4)_2$. In a typical experiment, $[Ni(P^{Ph}_2N^{PhOMe}_2)_2(CH_3CN)](BF_4)_2$ (15 mg, 0.012 mmol) and *p*-anisidine (6.0 mg, 0.049 mmol) were dissolved in 0.5 mL of dry acetonitrile-d_3 and transferred to an NMR tube equipped with a septum. Hydrogen gas was bubbled through the solution for 20 min. After an additional 10 min, the sample was analyzed by ^1H and ^{31}P NMR spectroscopy. The weighted averages of the aromatic proton chemical shifts of *p*-anisidine/*p*-anisidinium were used to determine the ratio of acid to base for the reference, and the ratio of $[Ni(P^{Ph}_2N^{PhOMe}_2)_2(CH_3CN)]^{2+}$ to $[HNi(P^{Ph}_2N^{PhOMe}_2)_2]^+$ was determined by ^{31}P NMR spectroscopy. These ratios were then used to determine the equilibrium constant. The samples were run again after 24 h to ensure equilibration. For $[Ni(P^{Cy}_2N^{Ph}_2)_2(CH_3CN)](BF_4)_2$, *p*-bromoaniline was used as the base, and for $[Ni(P^{Ph}_2N^{Ph}_2)(P^{Cy}_2N^{Ph}_2)(CH_3CN)](BF_4)_2$, aniline was used as the base.

Reactivity toward $NBu_4HCO_2\cdot HCO_2H$: General Procedure for NMR Titration. In a glovebox, a solution of $[Ni(P^{Ph}_2N^{PhOMe}_2)_2(CH_3CN)](BF_4)_2$ (5.0 mg, 0.0038 mmol) in 0.4 mL of CD_3CN was prepared in a 4 mL vial and transferred to a standard NMR tube capped with a septum. A stock solution of $NBu_4HCO_2\cdot HCO_2H$ was prepared by dissolving 331 mg (0.99 mmol) in a second 4 mL vial with 0.3 mL of CD_3CN. Aliquots of the $NBu_4HCO_2\cdot HCO_2H$ solution (1.0 μL, 0.0033 mmol) were added to the NMR tube via a 10 μL gastight syringe. The NMR tube was shaken thoroughly, and ^1H and ^{31}P NMR spectra were acquired. This procedure was followed until all the starting material was consumed. The $^{31}P\{^1H\}$ NMR spectra are shown in the Supporting Information.

Electrocatalytic Formate Oxidation: Order with Respect to Formate. The catalyst was dissolved in a benzonitrile solution with 0.2 M NBu_4OTf to make a solution with a total volume of 1.0 mL and a final catalyst concentration of 1.0×10^{-3} M. The solution was purged with N_2 for 5 min, and an initial cyclic voltammogram was recorded. Aliquots of $NBu_4HCO_2\cdot HCO_2H$ were added, and cyclic voltammograms were recorded to determine catalytic currents. Plots of TOF vs $[NBu_4HCO_2\cdot HCO_2H]$ were used to determine the order with respect to formate (see eqs 11 and 12 and Figure 7). The peak current (i_p) is the observed current for the Ni(II/I) in the absence of formate. The catalytic current (i_{cat}) is the observed peak or plateau current observed in the presence of $NBu_4HCO_2\cdot HCO_2H$.

Electrocatalytic Formate Oxidation: Titration of $[Ni(P^{Ph}_2N^{PhOMe}_2)_2(CH_3CN)](BF_4)_2$ with $NBu_4HCO_2\cdot HCO_2H$ and DBU. $[Ni(P^{Ph}_2N^{PhOMe}_2)_2(CH_3CN)](BF_4)_2$ (6.5 mg, 0.005 mmol) was dissolved in a 5.0 mL volumetric flask with 0.2 M NBu_4OTf benzonitrile solution. In a 1.0 mL volumetric flask, $NBu_4HCO_2\cdot HCO_2H$ (333 mg, 1.0 mmol) and 1,8-diazabicyclo[5.4.0]undec-7-ene (DBU, 150 μL, 1.0 mmol) were dissolved in 0.2 M NBu_4OTf benzonitrile solution. Aliquots of the $NBu_4HCO_2\cdot HCO_2H$/DBU solution were added to 1.0 mL of the $[Ni(P^{Ph}_2N^{PhOMe}_2)_2(CH_3CN)](BF_4)_2$ stock solution in 5 equiv increments. Cyclic voltammograms were recorded to determine catalytic currents. Rates and TOF were similar to those of the $[Ni(P^{Ph}_2N^{PhOMe}_2)_2(CH_3CN)](BF_4)_2$ with $NBu_4HCO_2\cdot HCO_2H$ in the absence of DBU, specifically 10.6 s^{-1} with DBU vs 8.5 without DBU.

Electrocatalytic Formate Oxidation: Order with Respect to Catalyst. The order with respect to catalyst was determined by titration of a 0.15 M $NBu_4HCO_2\cdot HCO_2H$ solution with catalyst, both dissolved in benzonitrile with 0.2 M NBu_4OTf. The solution was purged with N_2 for 5 min, and an initial cyclic voltammogram was recorded. Aliquots of catalyst were added, and cyclic voltammograms were recorded to determine catalytic currents. Plots of i_{cat} vs [cat] were used to determine the order with respect to catalyst, as shown in Figure 8.

Bulk Electrolysis. A multineck conical flask was used for the bulk electrolysis experiment. A stainless steel mount was attached to one neck, and to this mount a cylinder of reticulated vitreous carbon was attached as the working electrode. Two of the other necks of the flask were fitted with glass tubes terminating with 7 mm Vycor frits (Princeton Applied Research). One tube was used for the reference electrode and the other tube for the counter electrode. Both were filled with electrolyte solutions (0.2 M NBu_4OTf in benzonitrile), and the reference cell contained a silver chloride-coated silver wire, whereas a Nichrome wire was used in the countercell. With the fittings attached, the cell had a total volume of 328 mL. The cell was filled with stock solutions of catalyst and $NBu_4HCO_2\cdot HCO_2H$ to give 20 mL of a solution that was 0.76 mM in $[Ni(P^{Ph}_2N^{PhOMe}_2)_2(CH_3CN)](BF_4)_2$, 0.086 M in $NBu_4HCO_2\cdot HCO_2H$, and 0.2 M in NBu_4OTf. Controlled-potential coulometry was performed at ~100 mV positive of the peak of the catalytic current. After 16.3 C of charge had passed, samples of the gas in the headspace of the flask were removed via a gastight syringe and analyzed by gas chromatography. The percentages of N_2 and CO_2 in the headspace were determined through calibration against gas standards of a known composition. From these data, 5.3 mol of CO_2 per mole of catalyst was produced, a current efficiency of 93 ± 5% was calculated for CO_2 production, and no H_2 was observed.

■ ASSOCIATED CONTENT

Supporting Information. Crystallographic structure for $NBu_4HCO_2\cdot HCO_2H$ and crystallographic data and CIF files for $NBu_4HCO_2\cdot HCO_2H$, $[Ni(P^{Ph}_2N^{PhOMe}_2)_2(CH_3CN)]^{2+}$, $[Ni(P^{Cy}_2N^{Ph}_2)_2(CH_3CN)]^{2+}$, $[Ni(P^{Cy}_2N^{Ph}_2)(CH_3CN)_2]^{2+}$, $[Ni(P^{Cy}_2N^{Ph}_2)(P^{Ph}_2N^{Ph}_2)(CH_3CN)]^{2+}$, and $[Ni(P^{Ph}_2N^{PhOMe}_2)_2]$; $^{31}P\{^1H\}$ NMR spectra of the reactions of $[Ni(P^{Ph}_2N^{PhOMe}_2)_2(CH_3CN)]^{2+}$, $[Ni(P^{Cy}_2N^{Ph}_2)_2(CH_3CN)]^{2+}$, and $[Ni(P^{Cy}_2N^{Ph}_2)(P^{Ph}_2N^{Ph}_2)(CH_3CN)]^{2+}$ with $NBu_4HCO_2\cdot HCO_2H$; detailed synthetic procedure for $[Ni(P^{Ph}_2N^{PhOMe}_2)_2(CH_3CN)]^{2+}$. This material is available free of charge via the Internet at http://pubs.acs.org.

■ AUTHOR INFORMATION

Corresponding Author
aaron.appel@pnl.gov; ckubiak@ucsd.edu

■ ACKNOWLEDGMENT

Funding by Deutsche Forschungsgemeinschaft (J.S.), the NSF GRFP (C.S.), and by the Helios Solar Energy Research Center, which is supported by the Director, Office of Science, Office of Basic Energy Sciences of the U.S. Department of Energy under Contract No. DE-AC02-05CH11231, is gratefully acknowledged. B.R.G., J.C.L., A.M.A., and D.L.D. were supported by the U.S. Department of Energy, Office of Science, Office of Basic Energy Sciences, Division of Chemical Sciences, Biosciences and Geosciences. J.A.S.R., M.L.H., U.J.K., and J.Y.Y. were supported as part of the Center for Molecular Electrocatalysis, an Energy Frontier Research Center funded by the U.S. Department of Energy, Office of Science, Office of Basic Energy Sciences, under FWP 56073. Pacific Northwest National Laboratory is operated by Battelle for the U.S. Department of Energy.

REFERENCES

(1) *A Modular Approach to the Development of Molecular Electrocatalysts for H2 Oxidation and Production Based on Inexpensive Metals*; Wiley-VCH: Weinheim, 2010; pp 165−180.

(2) Rice, C.; Ha, S.; Masel, R. I.; Wieckowski, A. *J. Power Sources* **2003**, *115*, 229–235.

(3) Song, C. *Catal. Today* **2002**, *77*, 17–49.

(4) Zhu, Y.; Ha, S. Y.; Masel, R. I. *J. Power Sources* **2004**, *130*, 8–14.

(5) Reutemann, W., ; Kieczka, H. *Formic Acid−Ullmann's Encyclopedia of Industrial Chemistry*; Wiley-VCH: Weinheim, 2002.

(6) Reda, T.; Plugge, C. M.; Abram, N. J.; Hirst, J. *Proc. Natl. Acad. Sci. U.S.A.* **2008**, *105*, 10654–10658.

(7) Enthaler, S.; von Langermann, J.; Schmidt, T. *Energy Environ. Sci.* **2010**, *3*, 1207–1217.

(8) Fellay, C.; Dyson, P. J.; Laurenczy, G. *Angew. Chem., Int. Ed.* **2008**, *47*, 3966–3968.

(9) Fraze, K.; Wilson, A. D.; Appel, A. M.; Rakowski DuBois, M.; DuBois, D. L. *Organometallics* **2007**, *26*, 3918–3924.

(10) Rakowski DuBois, M.; DuBois, D. L. *Chem. Soc. Rev.* **2009**, *38*, 62–72.

(11) (a) DuBois, D. L.; Berning, D. E. *Appl. Organomet. Chem.* **2000**, *14*, 860–862. (b) Curtis, C. J.; Miedaner, A.; Ellis, W. W.; DuBois, D. L. *J. Am. Chem. Soc.* **2002**, *124*, 1918–1925.

(12) Wilson, A. D.; Newell, R. H.; McNevin, M. J.; Muckerman, J. T.; Rakowski DuBois, M.; DuBois, D. L. *J. Am. Chem. Soc.* **2006**, *128*, 358–366.

(13) Märkl, V.; Jin, G. Y.; Schoerner, C. *Tetrahedron Lett.* **1980**, *21*, 1409–1412.

(14) Kane, J. C.; Wong, E. H.; Yap, G. P. A.; Rheingold, A. L. *Polyhedron* **1999**, *18*, 1183–1188.

(15) Bobrov, S. V.; Karasik, A. A.; Sinyashin, O. G. *Phosphorus Sulfur and Silicon and the Related Elements* **1999**, *146*, 289–292.

(16) Kilgore, U. J.; Roberts, J. A. S.; Pool, D. H.; Appel, A. M.; Stewart, M. P.; Rakowski DuBois, M.; Dougherty, W. G.; Kassel, W. S.; Bullock, R. M.; DuBois, D. L. *J. Am. Chem. Soc.* **2011**, *133*, 5861–5872.

(17) Yang, J. Y.; Bullock, R. M.; Dougherty, W. G.; Kassel, W. S.; Twamley, B.; DuBois, D. L.; DuBois, M. R. *Dalton Trans.* **2010**, *39*, 3001–3010.

(18) González-Arellano, C.; Gutiérrez-Puebla, E.; Iglesias, M.; Sánchez, F. *Eur. J. Inorg. Chem.* **2004**, 1955–1962.

(19) Drew, J.; Hursthouse, M. B.; Thornton, P. *J. Chem. Soc., Dalton Trans.* **1972**, 1658–1660.

(20) Nagataki, T.; Tachi, Y.; Itoh, S. *Chem. Commun.* **2006**, 4016–4018.

(21) Burling, S.; Elliott, P. I. P.; Jasim, N. A.; Lindup, R. J.; McKenna, J.; Perutz, R. N.; Archibald, S. J.; Whitwood, A. C. *Dalton Trans.* **2005**, 3686–3695.

(22) Miedaner, A.; Haltiwanger, R. C.; DuBois, D. L. *Inorg. Chem.* **1991**, *30*, 417–427.

(23) Raebiger, J. W.; Miedaner, A.; Curtis, C. J.; Miller, S. M.; Anderson, O. P.; DuBois, D. L. *J. Am. Chem. Soc.* **2004**, *126*, 5502–5514.

(24) Nimlos, M. R.; Chang, C. H.; Curtis, C. J.; Miedaner, A.; Pilath, H. M.; DuBois, D. L. *Organometallics* **2008**, *27*, 2715–2722.

(25) Curtis, C. J.; Miedaner, A.; Ciancanelli, R.; Ellis, W. W.; Noll, B. C.; Rakowski DuBois, M.; DuBois, D. L. *Inorg. Chem.* **2003**, *42*, 216–227.

(26) Berning, D. E.; Noll, B. C.; DuBois, D. L. *J. Am. Chem. Soc.* **1999**, *121*, 11432–11447.

(27) Wayner, D. D. M.; Parker, V. D. *Acc. Chem. Res.* **1993**, *26*, 287–294.

(28) Yang, J. Y.; Bullock, R. M.; Dougherty, W. G.; Kassel, W. S.; Twamley, B.; DuBois, D. L.; Rakowski DuBois, M. *Dalton Trans.* **2010**, *39*, 3001–3010.

(29) Yang, J. Y.; Bullock, R. M.; Shaw, W. J.; Twamley, B.; Fraze, K.; Rakowski DuBois, M.; DuBois, D. L. *J. Am. Chem. Soc.* **2009**, *131*, 5935–5945.

(30) Berning, D. E.; Miedaner, A.; Curtis, C. J.; Noll, B. C.; Rakowski DuBois, M. C.; DuBois, D. L. *Organometallics* **2001**, *20*, 1832–1839.

(31) Appel, A. M.; Pool, D. H.; O'Hagan, M.; Shaw, W. J.; Yang, J. Y.; Rakowski DuBois, M.; DuBois, D. L.; Bullock, R. M. *ACS Catal.* **2011**, *1*, 777–785.

(32) Yonker, C. R.; Linehan, J. C. *J. Organomet. Chem.* **2002**, *650*, 249–257.

(33) Yonker, C. R.; Linehan, J. C. *Prog. Nucl. Magn. Reson. Spectrosc.* **2005**, *47*, 95–109.

(34) Nicholson, R. S.; Shain, I. *Anal. Chem.* **1964**, *36*, 706–723.

(35) Saveant, J. M.; Vianello, E. *Electrochim. Acta* **1965**, *10*, 905–920.

(36) Savéant, J. M.; Vianello, E. *Electrochim. Acta* **1967**, *12*, 629–646.

(37) Izutsu, K. (International Union of Pure and Applied Chemistry, Commission on Electroanalytical Chemistry). *Acid−base dissociation constants in dipolar aprotic solvents*; Blackwell Scientific: Oxford, 1990.

(38) Kaljurand, I.; Kutt, A.; Soovali, L.; Rodima, T.; Maemets, V.; Leito, I.; Koppel, I. A. *J. Org. Chem.* **2005**, *70*, 1019–1028.

(39) Boddien, A.; Loges, B.; Junge, H.; Beller, M. *ChemSusChem* **2008**, *1*, 751–758.

(40) Morris, D. J.; Clarkson, G. J.; Wills, M. *Organometallics* **2009**, *28*, 4133–4140.

(41) Himeda, Y. *Green Chem.* **2009**, *11*, 2018–2022.

(42) Himeda, Y.; Miyazawa, S.; Hirose, T. *ChemSusChem* **2011**, *4*, 487–493.

(43) Sheldrick, G. M. *SHELXL 97*—Programm fur die Verfeinerung von Kirstallstrukturen; Universitat Gottingen, 1997.